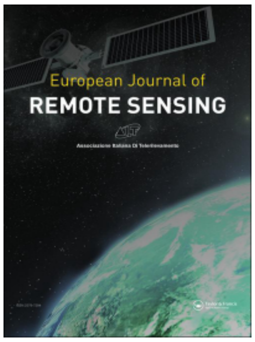

European Journal of Remote Sensing

ISSN: 2279-7254 (Online) Journal homepage: www.tandfonline.com/journals/tejr20

Joint use of multi-temporal satellite interferometric and geotechnical data for monitoring and investigating the kinematics of an urbanized relict landslide

Francesco Barbadori, Saduni Melissa Dahanayaka, Matteo Del Soldato, Fabio Arrighetti, Tommaso Macciò, Roberto Macciò, Andrea Cevasco & Giacomo Pepe

To cite this article: Francesco Barbadori, Saduni Melissa Dahanayaka, Matteo Del Soldato, Fabio Arrighetti, Tommaso Macciò, Roberto Macciò, Andrea Cevasco & Giacomo Pepe (2026) Joint use of multi-temporal satellite interferometric and geotechnical data for monitoring and investigating the kinematics of an urbanized relict landslide, European Journal of Remote Sensing, 59:1, 2620877, DOI: 10.1080/22797254.2026.2620877

To link to this article: https://doi.org/10.1080/22797254.2026.2620877

Published online: 28 Jan 2026.

EUROPEAN JOURNAL OF REMOTE SENSING
2026, VOL. 59, NO. 1, 2620877
https://doi.org/10.1080/22797254.2026.2620877

RESEARCH ARTICLE

Joint use of multi-temporal satellite interferometric and geotechnical data for monitoring and investigating the kinematics of an urbanized relict landslide

Francesco Barbadori[a], Saduni Melissa Dahanayaka[a], Matteo Del Soldato[a], Fabio Arrighetti[b], Tommaso Macciò[b], Roberto Macciò[b], Andrea Cevasco[c] and Giacomo Pepe[c]

[a]Department of Earth Sciences, University of Florence, Florence, Italy; [b]Private Consultant, Albenga, Savona, Italy; [c]Department of Earth, Environment and Life Sciences, University of Genoa, Genoa, Italy

ABSTRACT

The residual kinematics of relict landslides involving built areas can represent a severe source of risk. Such slope movements can be monitored through ground-based geotechnical and remote sensing techniques, like interferometric synthetic aperture radar (InSAR). In this study, to investigate the residual slow movements of a relict landslide affecting the Mendatica village (Liguria, NW Italy), a coupled analysis of multi-temporal displacement monitoring datasets from slope inclinometers and InSAR (ERS, RADARSAT, ENVISAT, COSMO-SkyMed and Sentinel-1) was performed. Owing to the favorable satellite acquisition geometry and a rather continuous temporal efficiency of in situ geotechnical equipment, the study emphasized the complementariness between the two techniques. The joint analysis allowed reconstructing the patterns of movement over almost 30 years. Furthermore, by exploiting the spatial correspondence and long temporal overlap of InSAR and geotechnical measurements, together with geomorphological evidence, the displacement components were combined to reconstruct the subsurface geometric structure and the kinematic model of the landslide. The results revealed that the residual landslide activity consists of composite movements involving major translational movements coupled with weak rotational mechanisms, mainly driven by erosion at the landslide toe. The study outcomes represent useful knowledge for the zonation of movement intensity for medium-to-long term landslide risk management strategies.

ARTICLE HISTORY
Received 30 June 2025
Revised 29 October 2025
Accepted 19 January 2026

KEYWORDS
Synthetic aperture radar; geotechnical monitoring; landslide kinematics; relict landslide; slope inclinometer

Introduction

Landslides represent one of the major natural risks for the population worldwide (Kjekstad & Highland, 2009; Turner, 2018) since their impacts can cause loss of human lives, social and economic losses, and disruption of structures and infrastructures. Italy, with almost 35% of its territory occupied by hilly-mountainous environments, presents a high number (>600,000) of active and dormant landslides (Iadanza et al., 2021; Trigila et al., 2010, 2021). Thanks to the availability of interferometric Sentinel-1 data combined with ENVISAT data, Confuorto et al. (2023) assessed the state of activity of most of them. Several landslides are monitored at the slope scale to investigate their kinematic evolution and to forecast acceleration trends and/or the initiation time (e.g. Cenni et al., 2021; Hervás et al., 2003).

At the slope scale, the most common equipment used for landslide displacement monitoring consists of *in situ* geotechnical (e.g. inclinometers and extensometers) and geodetic (e.g. GNSS stations) tools, owing to their accuracy in detecting movements downslope and orthogonal components (i.e. North–South and East–West direction). Among the others, slope inclinometers are the most effective in determining the magnitude, rate, direction and depth of subsurface horizontal displacements (Bordoni et al., 2023; Stark & Choi, 2008). Indeed, this device detects the initiation and evolution of deformation normal to the axis of a flexible casing tube installed within a vertical borehole by means of a probe that measures an angle of

CONTACT Saduni Melissa Dahanayaka melissa.dahanayaka@unifi.it Department of Earth Sciences, University of Florence, via G. la Pira 4, 50121 Florence, Italy

inclination at regular depth intervals. The examination of time-series of subsurface horizontal deformations allows the collection of important data aimed at understanding the geometry and state of activity of a landslide. However, the implementation of an inclinometric monitoring network can be cost- and time-consuming, requiring careful operations during both the installation and measuring phases (Stark & Choi, 2008). Moreover, either at sites with rugged morphology (i.e. with scarce and/or difficult accessibility) or in urbanized contexts, the installation of inclinometers can be limited by logistic constraints because of the difficulties in drilling boreholes. These factors can affect both the spatial and temporal resolution of subsurface displacement data, hampering the investigation of the kinematic-geometric landslide features.

With the evolution in technologies applied to landslide monitoring and mapping, from more than two decades, remote sensing data have begun to be effectively used for landslide monitoring, both at regional (Raspini et al., 2018) and slope scale (Song et al., 2021; Tofani et al., 2013; Yu et al., 2023). Synthetic aperture radar (SAR) data is extensively used to detect, map and monitor landslides and to create or update landslide inventories (Mondini et al., 2021; Novellino et al., 2024; Rosi et al., 2018; Solari et al., 2020). The application of SAR for landslide monitoring lies in the use of radar phase images and in the assessment of its variation between consecutive images, allowing the detection and monitor ground deformations over time. In the early 2000s, advanced interferometric methodologies, such as PSInSAR (Colesanti et al., 2003; Ferretti et al., 2001), enabled the investigation of ground deformation from extremely to very slow (e.g. Jiaxuan et al., 2020) by processing SAR images and focusing on high coherence points inside the radar image defined as persistent scatterers (PS) (e.g. buildings, bare rocks and infrastructures) to build up velocity maps of the area and time series of local cumulated displacement. In the following years, several algorithms were developed (Crosetto et al., 2016), including the small baseline subset InSAR (SBAS) (Berardino et al., 2002; Lopez-Quiroz et al., 2009) and others (e.g. Costantini et al., 2008; Costantini et al., 2014; Duro et al., 2004). An evolution of the PSInSAR technique, called SqueeSAR (Ferretti et al., 2011), introduced the concept of Distributed Scatterers (DS) to enhance the spatial measurement density. InSAR technique provides higher density measurement points (MPs) and a lower annual cost per measuring point (MP) than GNSS, extensometers and other *in situ* techniques (Tomás et al., 2014). However, despite its strengths, several limitations can affect the spatial and temporal completeness of this data. One major constraint is the availability of high-resolution imagery, which can limit the detection of small-scale deformation features, particularly in complex terrains or urban environments. Additionally, InSAR relies on the presence of stable radar scatterers; therefore, areas with dense vegetation, water bodies, or building-free surfaces often exhibit low coherence, resulting in data gaps and reduced measurement accuracy. Temporal decorrelation due to changes in surface properties between acquisitions further degrades the quality of interferograms, especially in vegetated regions where rapid growth or seasonal variations occur. Finally, the revisit time of satellite platforms and the viewing geometry impose constraints on the temporal resolution and the ability to detect deformation along certain directions, which may lead to underestimation of displacement in areas with complex three-dimensional movement (Meisina et al., 2008; Moretto et al., 2021).

In order to balance the advantages and constraints of ground-based and remote sensing monitoring methods, several scientific papers explored the joint use of inclinometric and SAR data proposing complementary approaches for: (i) investigating the kinematics and/or damage evolution of slow-moving landslides (e.g. Calò et al., 2012, 2014; Del Soldato et al., 2018; Journault et al., 2018; Peduto et al., 2021; Tofani et al., 2013), (ii) reconstructing the kinematic and geometry of coastal landslides (e.g. Cevasco et al., 2018; Uzielli and Catani, 2015) and (iii) assessing the effectiveness of structural risk mitigation measures (Bru et al., 2024; Confuorto et al., 2019, Di Maio et al., 2018). However, the use of long-term contemporary data series is quite uncommon in the literature, mainly because of efficiency issues affecting *in situ* geotechnical equipment. Moreover, for mapping and reconstructing historical slope deformation trends, remotely sensed data provided by ERS, RADARSAT (RST), ENVISAT (ENV) and COSMO-SkyMed (CSK) missions have been commonly used. In recent years, Sentinel-1 (SNT) constellation has provided continuous and ongoing data for land deformation monitoring purposes (Torres et al., 2012). The integration of these latter SAR datasets with long-term geotechnical subsurface monitoring is still of relevant interest in the field of research on landslides (Refice et al., 2019; Wasowski & Pisano, 2020), especially concerning the comprehension of the kinematics of large and deep-seated relict landslides. According to the technical literature (Lopez Saez et al., 2012; Mather et al., 2003; WP/WLI, 1993), these mass movements are described as inactive landslides whose primary evolutionary stages developed under climatic and geomorphological conditions considerably different from those at present. Although the original movement mechanisms are no longer active, the relative stability of the landslide volume can be punctuated by localized reactivations or residual movements, producing hazard scenarios that are often a source of severe damage on the built environment (Cevasco et al., 2018). However, owing to the complex geomorphological, hydrogeological and engineering-geological settings characterizing relict landslides, the investigation of instability mechanisms and their temporal evolution is seldom straightforward. For these reasons, the use of integrated and multitemporal monitoring approaches plays a key role in the framework of landslide risk management.

In this work, a back analysis of the slope movements affecting the Mendatica village (western Liguria Region, NW Italy) through the coupled use of slope inclinometers and interferometric data is presented. This village is settled on the accumulation zone of one of the largest deep-seated and urbanized relict landslides of the Liguria Region. The residual kinematics that still affects this portion of the landslide involves active slow movements with occasional acceleration or reactivation episodes (Pepe et al., 2021) that caused massive damage to infrastructure and buildings over the past decades, in some cases forcing inhabitants to be evacuated. Previous studies dealt with the movement dynamics affecting this village during some significant periods using either ground-based (Cevasco and Pepe, 2016; Pepe et al., 2021) or satellite (Notti, Herrera et al., 2014) displacement data. However, no thorough investigations of landslide motion over long-term time spans with coupled employment of *in situ* and remotely sensed data are still available. Since 2006, a geotechnical monitoring system consisting of slope inclinometers and piezometers has been implemented inside the village of Mendatica and its outskirts. Regarding remote measurement of displacements, data from ERS, ENV, RST, CSK and SNT missions were used, enabling the investigation of slope movements from 1992 to 2021. The long-term temporal overlap between subsurface geotechnical data and satellite datasets is expected to contribute to a better understanding of the deformation patterns as well as the nature of the movement mechanisms threatening the urban environment.

Study area

The study area is located in the uppermost part of the Arroscia Basin in the western portion of the Liguria Region (Imperia Province, NW of Italy) (Figure 1). From the geological point of view, this portion of the region belongs to the frontal segment of the Ligurian Alps, a fold-and-thrust belt, here characterized by thick Cretaceous non-metamorphic turbiditic deposits pertaining to the Piedmont-Oceanic Domain (Figure 1), also known in the literature as the Western Liguria Flysch complex (Decarlis et al., 2013; Giammarino et al., 2010). The study area is characterized by the tectonic piling of the Sanremo–Monte Saccarello Unit and the Moglio–Testico Unit. The outcropping rocks belong to the following three formations (bottom to top): Testico Fm. (Moglio–Testico Unit, Lower Cretaceous-early Upper Cretaceous), San Bartolomeo Fm. (Sanremo–Monte Saccarello Unit, Upper Hauterivian–Upper Campanian) and Bordighera Sandstones Fm. (Sanremo–Monte Saccarello Unit, Upper Campanian–Maastrichtian) (Figure 1). The first formation is represented here by the Pieve di Teco Member, which outcrops with irregular, from thin to medium stratified, sequences of marls, calcareous marls and sandy marls. The other two geological formations are mainly composed of thinly bedded varicoloured shales and medium- to thick-bedded siliciclastic sandstones, respectively (Maino & Seno, 2016).

The Mendatica relict landslide is a mass movement of large dimensions developing along an entire east-facing slope (Figure 1). The dimensions of the displaced mass are over 2.5 km in length along the longitudinal axis, with a maximum width of approximately 950 m, and an extension greater than 2.0 km^2. The northern and eastern flanks of the landslide body are bordered by the paths of two streams, while the southern flank is limited by the left side of an east-west oriented ridge. Like many relict landslide systems, many original morphological features are no longer clearly recognizable since they are widely obliterated by denudational processes, internal deformation, successive mass movements, vegetation cover and human activity. The main crown is located at an elevation of approximately 1700–1800 m a.s.l.; below, the main scar is still visible, albeit densely vegetated. The landslide toe is situated at 600–625 m a.s.l. and, both to the left and right, is affected by the erosion operated by the Passo Cagnasso and Arroscia streams, respectively.

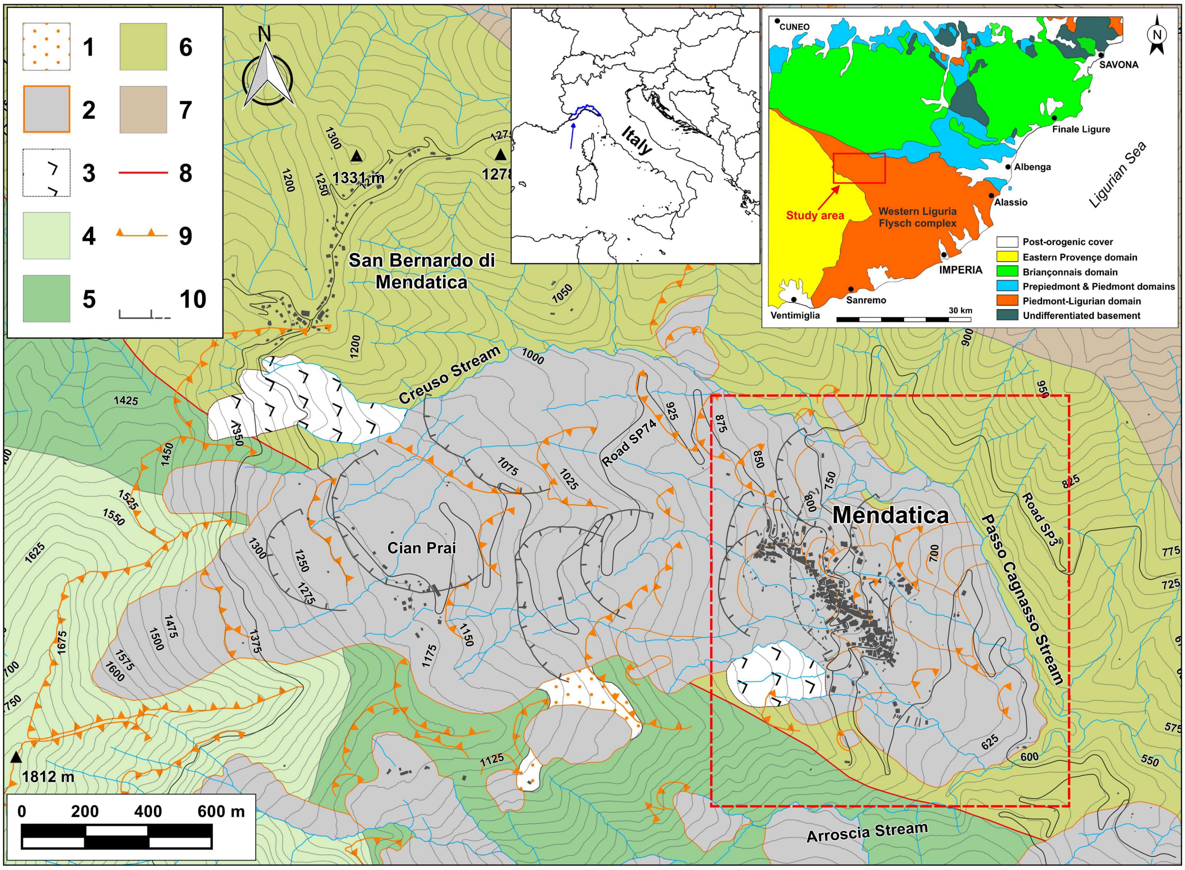

Figure 1. Geological and geomorphological map of the study area: (1) slope debris; (2) landslide body; (3) rockslide (presumed); (4) Bordighera Sandstones Fm.; (5) San Bartolomeo Fm.; (6) Testico Fm.–Pieve di Teco Member; (7) Moglio Shales Fm.; (8) tectonic contact; (9) landslide scarp; (10) head of rotational slide/buried (redrawn and modified after Federici et al. (2007)).

The internal morphology of the landslide body shows an undulated topography characterized by a series of depletion areas and scarps, most likely related to secondary and/or subsequent mass movements. Moreover, the entire displaced mass is partly dissected by a disjointed internal drainage pattern showing small and linear channels. The several morphological elements associated with primary movement are considered inactive or dormant. Neither geomorphological indicators nor documented information on stability issues are known in the middle and upper part of the main landslide body. However, residual landslide activity still affects some portions of the landslide foot hosting the hamlet of Mendatica, which was prevalently built along a gently pronounced and NW-SE-oriented morphological hump. Here, historical information on damage is repeatedly documented from the early 1970s onwards (e.g. 1970, 1976, 1977, 1985, 1993, 1994, 2000 and 2013) (Federici et al., 2007; Pepe et al., 2021). In particular, the eastern sector of the village suffered from extensive damage due to the active slope movements that have occurred over the last 20 years. Starting from 2006, several remedial works aimed at mitigating the extent of ground-instabilities have been carried out by public authorities, chiefly consisting of impermeable stream bed and bank revetments, automatic deep drainage systems and subhorizontal drains. To support the design of remedial measures, several stratigraphic drillings were executed in the last 18 years. Based on the outcomes of stratigraphic boreholes, in the sector of the village the landslide body shows thickness typically varying from approximately 20 m to 30 m. However, in some parts of the accumulation, the depth of the bedrock resulted as deep as 40 m, with maximum depths over 50 m (Pepe et al., 2021). A thorough analysis of core materials allowed to distinguish two main geotechnical horizons prevalently based on the granulometric features. The deepest one mainly consists of clayey and silty sands with gravel (SC, SM–SC according to the Unified Soil Classification System), and it is overlaid by a layer mostly composed of coarse-grained soils, chiefly silty and clayey gravels (GM and GC). The landslide deposit often shows marked spatial variations in granulometric and textural features along with the occurrence of chaotic fabrics. In this sector of the landslide accumulation, the bedrock consists of soft and fractured marls, clayey marls and sandy marls referring to the Pieve di Teco Member (Testico Fm.). Furthermore, in some drillings, at the contact interface between the landslide deposit and the bedrock, basal horizons made up of weak breccias were found.

Materials and methods

To reconstruct the long-term spatiotemporal evolution of the landslide displacements and to investigate the landslide kinematics, remote sensing InSAR data and ground-based geotechnical monitoring data were combined with geomorphological evidence (Figure 2). The ground instrumentation consists of several boreholes equipped with inclinometers. Subsurface displacement data were collected from previous scientific works (Cevasco and Pepe, 2016; Pepe et al., 2021) and from unpublished technical reports. In order to obtain as complete as possible time series, rainfall data were gathered from four different rain gauges: (i) before 2015, by the rain gauges installed at the villages of Pornassio, Colle di Nava and Piaggia, which are located within a maximum radius of approximately 6 km from the study area and (ii) since 2015, by a rain gauge installed over the active portion of the Mendatica landslide. Regarding InSAR data, different satellite constellations permitted displacement time series analysis from 1992 to the end of 2021.

Geotechnical data

A geotechnical monitoring network was installed in correspondence of the Mendatica village and its surroundings (Figure 3), which was composed of 29 boreholes equipped with flexible inclinometer casings or open-pipe piezometers. Generally, the casing tubes of inclinometers have been advanced more than 5 m below the interface between the landslide deposits and the firm bedrock (Stark & Choi, 2008). Inclinometer measurements cover a period of 15 years and were executed using a removable biaxial probe. This monitoring window can be split into two main monitoring campaigns because of a change of the measuring probe (Figure 3). Both monitoring surveys are characterized by variable reading frequencies. The first campaign started in December 2006 (i.e. zero reading) and ended in December 2016, involving a total of 15 measurements (Figure 3). During this first monitoring period, some tubes (i.e. S2, S5, S9, S12 and S13) went out of use due to the magnitude of deformations produced by the sharp accelerations of movements. These occurrences moved the local authorities to replace some verticals with new ones

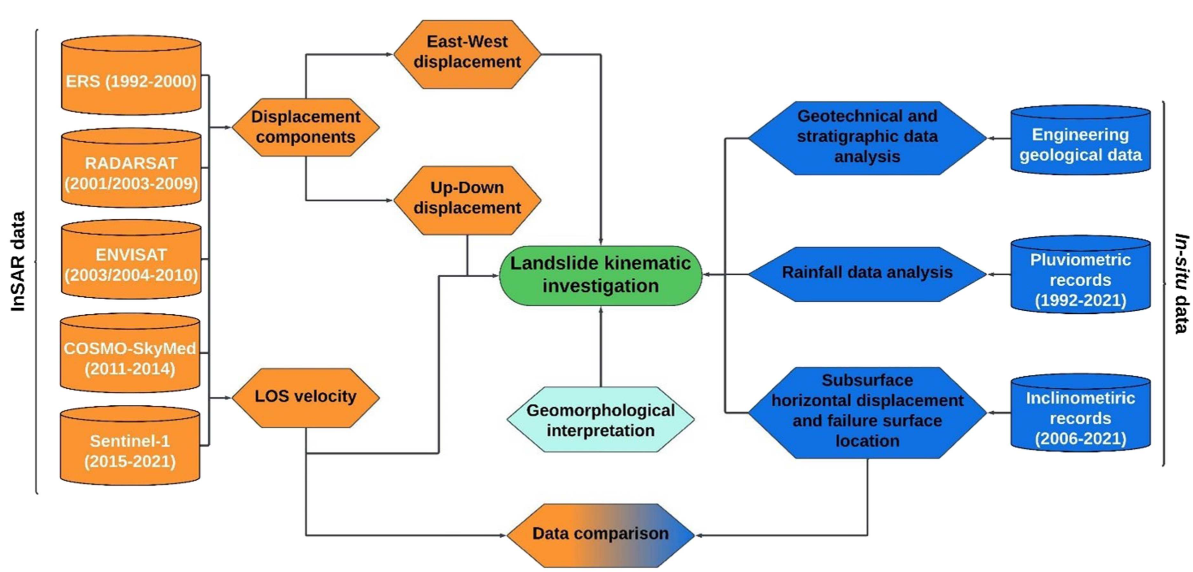

Figure 2. Flowchart of the study workflow.

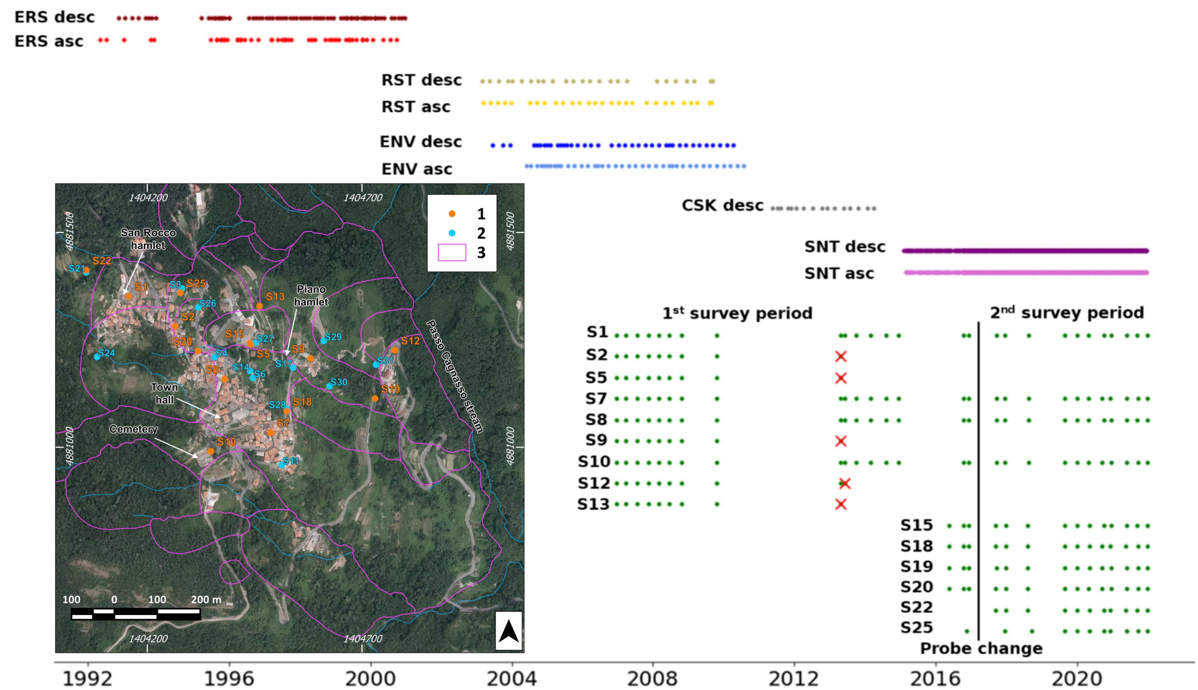

Figure 3. Temporal acquisition frequency of the InSAR satellites and geotechnical instruments used in this study (legend: (1) inclinometer; (2) piezometer; (3) landslide body; red crosses represent the datetime of inclinometer rupture).

through the execution of new core destruction boreholes (Figure 3). The second monitoring campaign started in September 2017, consists of ten measurements and is currently ongoing. In this work, the measurements performed until the end of 2021 were considered (Figure 3). Along tubes S1 and S8, traditional measurements were interrupted at mid-2020 because of the installation of automatic inclinometric probes. The surveys were executed starting from the bottom of the tubes up to the head of the casing tube while readings were acquired every 0.5-m interval. The use of two different probes implied the definition of two zero measurements at the beginning of the monitoring campaigns. The accuracy of the probe used during the first monitoring campaign was ±0.25 mm per reading and ±6 mm per 50 m of casing (Slope, 2006) while that of the second monitoring period had the following accuracy specifications: scale ±30°, resolution 25,000*sinα (where α = angle from vertical), non-linearity < ±0.057° in full scale. The acquired data were verified by checksums test to seek out measurement errors and evaluate their quality (Mikkelsen, 1996; Simeoni & Mongiovì, 2007). In order to gain insight into the movement mechanisms within the landslide volume, incremental subsurface horizontal displacements were used, as they were not affected by the progressive accumulation of systematic errors (Simeoni & Mongiovì, 2007; Simeoni et al., 2020). The cumulative local displacement vs. time profiles at the detected main active shear zones were used to determine the patterns and magnitudes of subsurface horizontal displacements (Mikkelsen, 1996). The average direction of the resultant movements has been used to build and depict on a planimetric view the displacement vectors (Stark & Choi, 2008). For comparison with interferometric SAR measurements, the resultant of incremental horizontal displacements was considered.

Satellite data

The datasets from 1992 to the end of 2021 were considered (Figure 3). The InSAR data were analysed both in ascending and descending orbits, except for the CSK dataset, which is available for the descending orbit only (Table 1).

The first satellite radar data were derived by the radar images of the European Remote Sensing (ERS) mission, consisting of two twin SAR satellites (ERS-1 and ERS-2) working on the C-band, commissioned by the European Space Agency (ESA), with a revisiting time of 35 days (Attema et al., 1998). In 1995, the

Table 1. Main features of the available datasets of ERS, RADARSAT, ENVISAT, COSMO-SkyMED and Sentinel-1 satellite constellations used to study the temporal evolution of the Mendatica landslide (see text for the explanation of acronyms).

Satellite	Track number	Orbit	Temporal span	*n.* images	Source
ERS	29	Ascending	3 May 1992 27 September 2000	48	PCN
ERS	252	Descending	10 November 1992 22 December 2000	70	PCN
RST	290	Ascending	17 March 2003 24 August 2009	80	RL
RST	97	Descending	7 April 2001 4 September 2009	65	RL
ENV	301	Ascending	7 June 2004 26 July 2010	39	PCN
ENV	251	Descending	20 June 2003 9 April 2010	38	PCN
CSK	28	Descending	23 May 2011 28 March 2014	353	PCN
SNT	88	Ascending	20 February 2015 21 December 2021	360	EGMS
SNT	66	Descending	7 February 2015 20 December 2021	362	EGMS

RADARSAT-1 mission was launched by the Canadian space agency (C-band), with a revisiting time of 24 days, until 2013 (Thompson, 2015). In 2002, Environmental Satellite (ENVISAT) was launched by the ESA (C-band) with a revisiting time of 35 days (Bruzzi et al., 1995). The new missions for radar Earth observation (EO) measures involved the Italian Space Agency (ASI) X-band product CSK (Serva et al., 2015; Virelli et al., 2014) and the SNT constellation, which consists of two twin satellites (Sentinel-1A and Sentinel-1B), working on the C-band (Torres et al., 2012), with a revisiting time of 12 days per each satellites (until the dismissal of Sentinel-1B for technical issues in the early 2022). SNT satellites offer high temporal resolution and open-access data, significantly advancing emergency response and InSAR-based land monitoring applications (e.g. for landslides and subsidence) (Geudtner et al., 2014; Torres et al., 2012).

The datasets from ERS, ENVISAT and CSK satellites were downloaded from the Portale Cartografico Nazionale (PCN – www.pcn.miniambiente.it) (Costantini et al., 2017); the RST dataset was available from the Regione Liguria database (RL), while the SNT data was downloaded from the EGMS (European Grund Motion Service), a pan European land monitoring service inside the Copernicus Land Monitoring System (CLMS), under the European Environment Agency (EEA), by the use of the EGMStream app (Festa & Del Soldato, 2023).

The datasets from ERS-1/2 and ENV, covering the 1992–2000 and 2002–2010 periods, respectively, were processed using the PSInSAR (Ferretti et al., 2001) and PSP-IFSAR (Costantini et al., 2009) approaches. The RST dataset covering the period 2001–2009 was instead processed using the SqueeSAR algorithm (Ferretti et al., 2011). From 2011 to 2014, the available data was the products derived by the processing of CSK images, which were available only in the descending orbit and processed using the coherence pixel technique (CPT) developed by the Remote Sensing Laboratory (RSLab), Universitat Politècnica de Catalunya, Spain (Blanco-Sanchez et al., 2008; Iglesias et al., 2015; Mora et al., 2003). The Sentinel-1 data from the European Ground Motion Service (EGMS) cover the period 2015–2021. The SNT data over Europe were elaborated using the following algorithms: (i) PSP-IFSAR (Costantini et al., 2009), (ii) SqueeSAR (Ferretti et al., 2011) and (iii) GSAR-GTSI (Prats-Iraola et al., 2012; Sansosti et al., 2006), performed with an integrated wide area processor (IWAP) (Eineder, 2003; Yagüe-Martínez et al., 2016). The EGMS provides three levels of products: (i) Level-2A (or basic product), which includes deformation maps and deformation time series along the radar LOS both for ascending and the descending orbit, referred to as a local reference point; (ii) Level-2B (or calibrated product), which includes deformation maps and time series combined with a reference GNSS network and measured along the LOS both for ascending and the descending orbit and (iii) Level-3 (or ortho product), which includes the two main deformation components (east–west and up–down components) inside a 100 m resampled point grid (Capes & Passera, 2022). The EGMS data became available in 2022 with the first baseline from

2015–2021 Sentinel-1 data (Costantini et al., 2021; Crosetto et al., 2020). All the data (from Level-2B) are freely accessible and downloadable via the EGMS Explorer (https://egms.land.copernicus.eu/).

To reconstruct the deformation history of the landslide and to study its motion features, long time series covering the entire time span of the available interferometric data were built up. Three main sectors along the longitudinal axis of the landslide accumulation were selected. Specifically, the first and second landslide sector (i.e. LS1 and LS2) consist approximately the upper and middle portion of Mendatica village, respectively, while the third sector (i.e. LS3) encompasses the south-eastern outskirt of the town coinciding with the landslide foot. The definition of these sectors was guided by the spatial distribution of inclinometers and by previous information on movement-induced damage available from previous works and historical information (Federici et al., 2007; Pepe et al., 2021). To build up the sample time series that can summarize the displacement over time for each selected sector of the unstable slope, in both the ascending and descending geometries, data from single and high coherence MPs were extracted. To maintain spatial correlation between the different interferometric datasets, points located close to each other were selected and put together in chronological order, filling the gaps between the different datasets by a linear interpolation method. The most important available information on significant damage due to severe accelerations, reactivations and on the implementation of structural risk mitigation measures was highlighted on displacement time-series to investigate possible correlations with changes in displacement trends.

Joint analysis of monitoring data

The availability of terrain deformation measures from both *in situ* and remote sensing techniques for wide periods (i.e. >15 years) across the whole monitoring window (Figure 3) made it possible to compare these two datasets to explore their degree of correspondence. The interferometric data in both geometries were compared with the resultant of sub-surface horizontal displacements measured by the inclinometers. Half-yearly inclinometric measurements from tubes S1 and S5–S15 pair were compared with interferometric data referring to the closest and coherent MP deriving from the different interferometric datasets. These verticals are those characterized by the longest subsurface displacement time series in proximity of high coherence MP. Furthermore, the different components of displacement obtained from InSAR data (i.e. Up–Down and East–West components) and the average annual rates of subsurface horizontal movements recorded by the inclinometers have been qualitative integrated and interpreted, with the support of geomorphological evidence, to reconstruct the kinematic model of the landslide. To cover the operational measurement period of the inclinometers, the horizontal and normal components of RST (2001–2009) and ENV (2003/2004–2010) data were calculated by projecting the SAR measurement vectors along the satellite LoS direction in both the ascending and descending orbit. For SNT, the components dataset was downloaded directly from the EGMS portal as Level-3 data (Ortho product). To process RST and ENV data and obtain East-West and vertical components, a spatial joint and vector-based approach was used (Notti, Meisina et al., 2014), in which MP data of both orbits were resampled into a common spatial grid with dimensions calibrated according to the interferometric data density (25 × 25 for RST and 50 × 50 for ENV). This allowed us to obtain a synthetic MP positioned at the centre of each cell of the grid and to calculate the average velocity values of all MP located within the cell. The East–West and vertical velocity components were calculated using the average velocities and direction cosines (calculated through the azimuth and the incidence angle of the LoS) of the SAR satellite for both the ascending and descending geometries. To cover the same time span and compare dataset from different satellites, ENV constellation dataset was processed to obtain normal and horizontal components. However, owing to the limited number of images compared to RST, despite the larger spatial grid size, the number of pseudo-MP obtained was insufficient for the purposes of interpretation.

Results

Inclinometric measurements

Profiles of incremental displacements measured along the inclinometric tubes during the first geotechnical monitoring campaign (i.e. from December 2006 to December 2016) coupled with simplified stratigraphic logs retrieved from core drilling operations are shown in Figure 4.

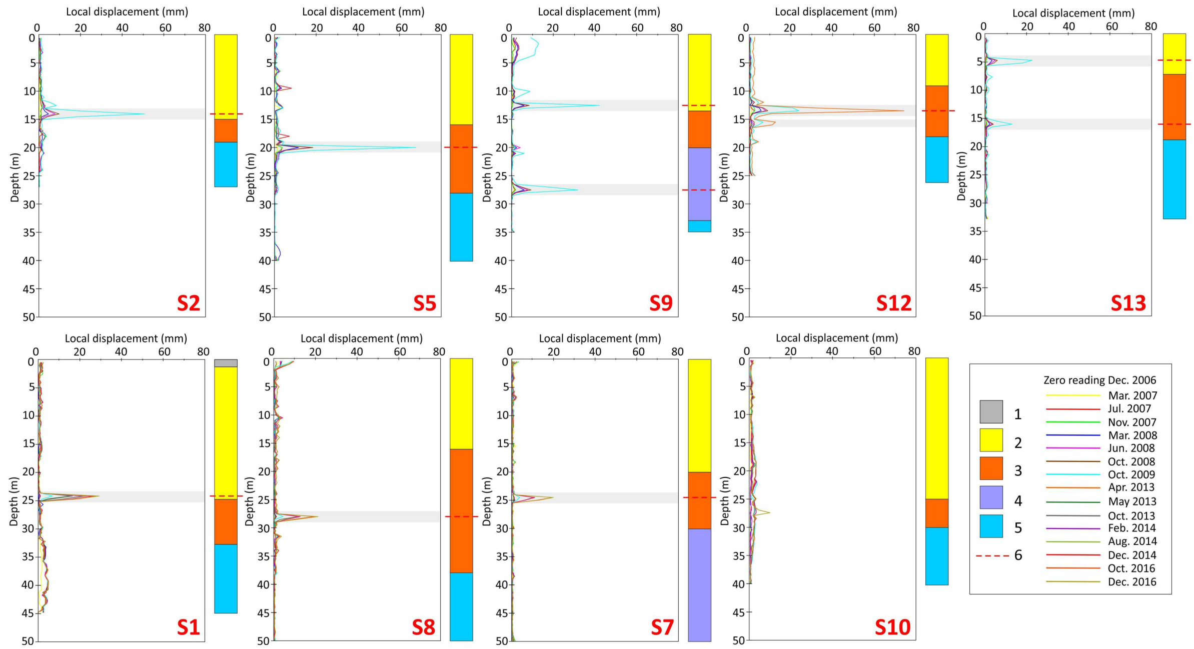

Figure 4. Incremental displacement profiles measured along the inclinometer tubes during the first geotechnical monitoring campaign (period December 2006–December 2016). Next to each graph, the corresponding simplified borehole stratigraphy is depicted (legend: (1) man-made fills; (2) silty gravels and clayey gravels; (3) silty and clayey sands; (4) weak breccias; (5) bedrock and (6) failure surface).

Except for tube S10, which recorded irregular and slight deformations throughout its height, all other local displacement profiles show sharp and well-defined spikes. Single main failure surfaces or major and secondary sliding levels can be noted, outlining that most of the subsurface horizontal displacements developed along localized failure bands at different depths within the landslide volume. The most significant active shear displacements resulted deep-seated, namely, in the depth range of 10.0–15.0 m and/or 20.0–30.0 m, depending on the tube. The deepest sliding zones were found from 25.5 m to 28.0 m below ground level (bgl), although rare cases of marked shallow deformations (up to 5 m deep) were observed (Table 2). Both above and below the most pronounced incremental displacement peaks, either negligible or slight local deformations (≤5 mm) were detected (Figure 4). Along the casing tube S13, considering the typical deep-seated nature of the movements detected in the other monitored verticals, the main failure surface was assumed to be that located at a depth of 16 m (Figure 4).

By comparing Figures 4 and 5, it can be noted that the outcomes of the second monitoring phase (i.e. from September 2017 to December 2021) are highly consistent with those of the previous phases. Indeed, the pre-existing main failure surfaces continued to be active, maintaining very similar features to those detected during the first monitoring window (e.g. compare the borehole profiles S1, S8 and S7). During the zero reading, the bottom of tubes S1 and S8 could no longer be reached; in fact, the new measurements were stopped at the depth of about 26.0 and 31.0 m, respectively (Figure 5).

Interestingly, even along the verticals drilled to replace the sheared-off inclinometer casings, namely, tubes S15 and S19, the same pre-existing failure zones were clearly detected (Tables 2 and 3). Similarly, along newly deployed monitoring verticals (i.e. boreholes S20 and S25), pronounced peaks of incremental displacements corresponding to localized deep-seated sliding surfaces were detected (Figure 5). Only shallow deformations were measured from inclinometer S18, while no relevant movements (i.e. below the system accuracy) were detected along vertical borehole S22, which is in the uppermost part of Mendatica village (see Figure 3). The results of the monitoring campaigns are also similar regarding the average azimuth of the movement vectors, which were mostly oriented in the E direction and in accordance with the dip direction of the slope, as shown in the topographic map depicted in Figure 6a. In this latter map, the location of the most significant structural risk mitigation works executed over the monitoring window is also reported.

Table 2. Summary of the main inclinometric data collected from 2006 to 2016.

		Main failure surface			Secondary failure surface		
Tube ID	Measurement period	Depth (m)	Cumulative displacement (mm)	Movement direction	Depth (m)	Cumulative displacement (mm)	Movement direction
S1	December 2006–December 2016	24.5	28.9	E	–	–	–
S2	December 2006–October 2009	14.0	50.0	E	–	–	–
S5	December 2006–October 2009	20.0	68.0	E	–	–	–
S7	December 2006–December 2016	25.5	15.6	S	–	–	–
S8	December 2006–December 2016	28.0	20.6	SE	–	–	–
S9	December 2006–October 2009	12.5	41.0	E	27.5	32.5	SE
S10	December 2006–December 2016	–	–	–	–	–	–
S12	December 2006–April 2013	13.5	71.0	E	15.5	5.1	E
S13	December 2006–October 2009	16.0	12.4	E	4.5	20.0	E

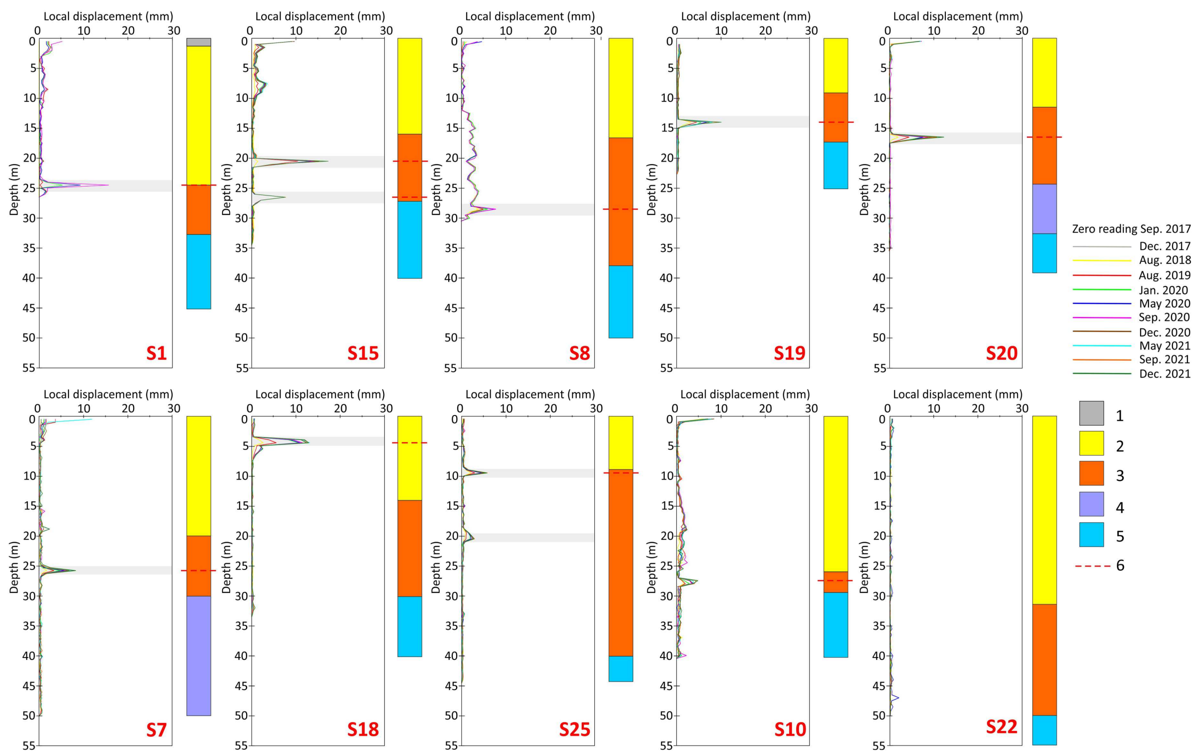

Figure 5. Incremental displacement profiles were measured along the inclinometer tubes during the second geotechnical monitoring campaign (period September 2017–December 2021). Next to each graph, the corresponding simplified borehole stratigraphy is depicted (legend: (1) man-made fills; (2) silty gravels and clayey gravels; (3) silty and clayey sands; (4) weak breccias; (5) bedrock and (6) failure surface).

By observing the time series of cumulative local displacements measured at the main failure surfaces (Figure 6a), different movement characteristics across the landslide accumulation can be noticed. Over the whole observation period, the most marked subsurface horizontal displacements took place either to the east or north-east of the outskirt of Mendatica (i.e. sectors LS2 and LS3). This is outlined by the maximum levels of cumulative local displacements reached along verticals S5 and S2 during the first monitoring campaign and subsequently along tubes S15 and S20 deployed to replace the previous ones (Figure 6b). The resultant incremental displacements were around 70 and 50 mm at tubes S5 and S2, respectively, corresponding to

Table 3. Summary of the main inclinometric data collected from 2017 to 2021.

		Main failure surface			Secondary failure surface		
Tube ID	Measurement period	Depth (m)	Cumulative local displacement (mm)	Movement direction	Depth (m)	Cumulative local displacement (mm)	Movement direction
S1	September 2017–April 2020	24.5	15.4	E	–	–	–
S7	September 2017–December 2021	25.5	7.8	S	–	–	–
S8	September 2017–April 2020	28.0	7.5	SE	–	–	–
S10	September 2017–December 2021	–	–	–	–	–	–
S15	September 2017–December 2021	20.5	16.7	E	26.5	7.5	E
S18	September 2017–December 2021	5.0	13.0	E	–	–	–
S19	September 2017–December 2021	14.0	10.0	E	–	–	–
S20	September 2017–December 2021	16.5	12.4	E	–	–	–
S22	September 2017–December 2021	–	–	–	–	–	–
S25	September 2017–December 2021	9.5	5.4	E	20.0	2.1	E

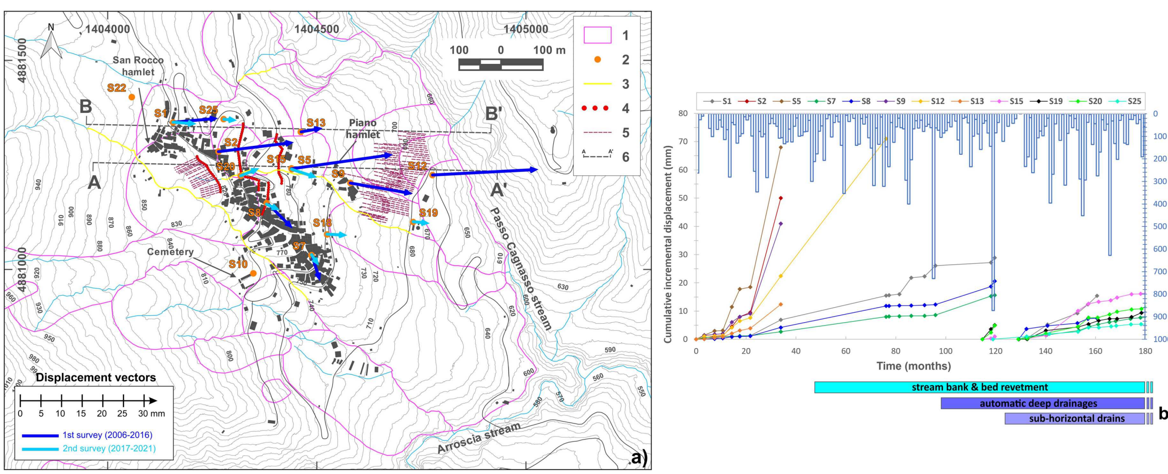

Figure 6. (a) Map of mean displacement vectors and implemented risk mitigation measures (legend: (1) landslide body; (2) inclinometer; (3) impermeable stream bed and bank revetment; (4) automatic drainage wells alignment; (5) subhorizontal drains; (6) traces of cross sections shown in Figure 12) and (b) cumulative local displacement profiles (related to the main slip surfaces) covering the period 2006–2021 together with monthly rainfall data and the indication of the periods during which the main risk mitigation measures have been implemented.

average movement velocities approximately between 15 and 25 mm/year (classifiable as "very slow" according to Cruden and Varnes, 1996). Displacements between 10 and 20 mm were measured at tubes S15 and S20 in the second monitoring window, reaching average annual rates lower than 5 mm/year (classifiable as "extremely slow" according to Cruden and Varnes, 1996). Meaningful deformations also affected verticals S12 and S19, especially during the first monitoring campaign, when subsurface horizontal displacements reached a peak of 71 mm, with an average yearly rate of 11 mm/year (i.e. "extremely slow" movements *sensu* Cruden and Varnes, 1996). Conversely, the extent of cumulative shear displacements measured along the inclinometers located in the south-western part of the village (e.g. tubes S7 and S8) was significantly lower during both survey time series.

The maximum measured cumulative local displacements were lower than 20 mm over approximately 10 years (i.e. duration of the first monitoring window), with average rates ≤2 mm/yr. In this sector, the temporal evolution of displacement was very similar during both survey time series, showing fairly constant movements alternated with substantially stable phases. Conversely, the patterns of movement detected in the inclinometers located within the most active parts of the landslide resulted rather differently. During the first survey time series, the profiles of cumulative shear displacement show the alternation of movement accelerations and decelerations (Figure 6b). The evidenced movement accelerations appear to be correlated with the most significant levels of monthly cumulative rainfall, which are usually greater than 300 mm. However, no clear evidence can be inferred due to the low temporal resolution of geotechnical measurements covering this survey period. On the other hand, the time trend of displacement for the second survey period did not show obvious signs of abrupt changes in movement rates. Despite the occurrence of monthly cumulative rainfall greater than 300 mm, with two peaks of almost 650 (i.e. in October 2020) and 900 mm (i.e. in November 2016), respectively, more uniform displacement trends were detected. Notably, the two rainfall peaks recorded in this period represent significant percentages of local average annual rainfall (i.e. around 1200 mm), and they are correlated to rainstorms characterized by short-duration and extremely high intensities. Indeed, at the Mendatica rain gauge, more than 540 mm over one day (October 2020 event) and two days (November 2016 event) were recorded.

Multitemporal InSAR data

The velocity maps of all the remote sensed datasets used in this study, including ascending and descending orbits as well as vertical (Up–Down) and horizontal (East–West) components, are shown in Figure 7.

Considering all the satellites constellations, differences emerge both temporally and spatially in MP density. More recent satellites (e.g. Sentinel-1) provide higher spatial coverage, yet a decrease in MP number from the upper parts of the slope (i.e. LS1 and LS2) towards the lower part of the landslide (i.e. LS3) is clearly visible. This difference is caused mainly by a higher density of buildings and infrastructure in the sectors of the landslide directly affecting the village, which act as existing reflectors, permitting to have more MPs.

Most of the MPs show mean velocity values within the stable range (±2 mm/year); nevertheless, areas with velocity values higher than the stable range are clearly visible (Figure 7). Two main zones consistently exhibit velocities above stability thresholds throughout the analysis period, with the highest values observed in the ascending orbit: (i) one is located in the eastern part of the landslide body (i.e. LS2), around inclinometers S5 and S15, where the football pitch, the school and the piano hamlet are located and (ii) the second is situated in the uppermost parts of the Mendatica village (i.e. LS1). The eastern slope portions of the urban area (i.e. LS2) present maximum velocity values of −14.5 mm/year (ERS dataset), −8.7 mm/year (RST dataset), 3.9 mm/year (ENV dataset) and 18.1 mm/year (SNT dataset). The northernmost outskirts of the village (i.e. LS1) present an increasing velocity trend, with maximum values of −4.9 mm/year (ERS dataset), −6.4 mm/year (RST dataset), −7.1 mm/year (ENV dataset) and −9.0 mm/year (SNT dataset). Notably, by analysing the deformation maps in the uppermost area of the village (i.e. San Rocco hamlet), a well-defined deformation spot is visible (Figure 7) moving from the RST and ENVISAT satellite datasets to the last available one, namely SNT. The LS3 sector of the landslide results in nearly "no displacement-affected" with velocity values inside the stable range (for the ERS and RST datasets) or slightly above (−2.8 in ENV dataset and −3.5 in SNT dataset). However, it should be noted that the scarce MP density in this landslide sector may affect a reliable detection of movements.

MP density for both the horizontal and vertical components vary across datasets, with the highest density observed in the RST dataset and the lowest in the ENV dataset. The East-West components present an increasing trend both regarding the displacement affected area and the displacement rates from RST to SNT dataset with maximum rates of 10 mm/year (RST dataset), 1.3 mm/year (ENV dataset) and 20.5 mm/year (SNT dataset), indicating that the eastward displacement rates range from extremely to very slow (Cruden and Varnes, 1996). The boxplots depicted in Figure 8 show the distribution of LoS displacement velocities derived from all satellite datasets in ascending and descending geometries for the whole landslide body. The plots highlight differences in median velocities and variability among the different constellations, with ERS showing larger dispersion and more negative outliers in the ascending mode; ENV and SNT exhibit narrower distributions and tighter interquartile ranges, respectively, while CSK descending data display a near-zero median with several localized outliers, reflecting its higher spatial resolution.

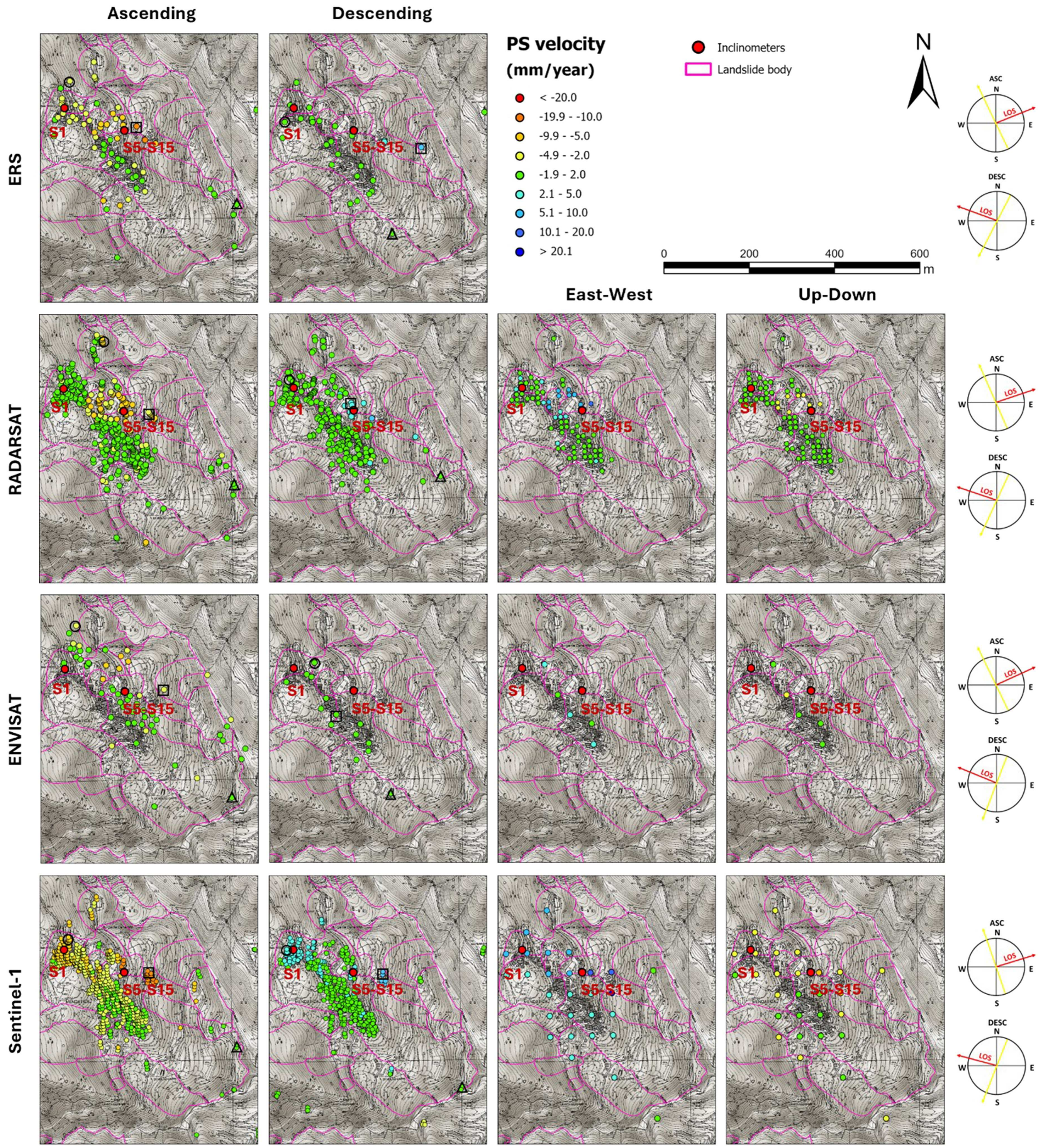

Figure 7. Velocity maps of the MPs located within the portion of the landslide body affecting the Mendatica village obtained from ERS, ENVISAT, RADARSAT and SNT datasets, in ascending and descending orbits along with East–West and Vertical components. Black geometry symbols represent MPs used to extract time series for the landslide sectors analysis: circles, squares and triangles indicate the selected upper (LS1), middle (LS2) and lower (LS3) sectors of Mendatica village, respectively. The position of inclinometers S1 and S5–S15 along with the azimuth angle representation of LoS are also shown.

Up–Down components show different spatial distributions across the various datasets (Figure 7). In particular, MPs from RST and ENV identify a clearly visible area located in the eastern part of the village with maximum rates of −3.2 mm/year (RST dataset) and −2.2 mm/year (ENV dataset), while data from Sentinel-1 detect a more spatially distributed displacement area, with a maximum velocity of −8.9 mm/year near the S5–S15 inclinometer pair. Also, these vertical component data highlight an increasing trend from RST to SNT, identifying a general downward movement with not very high rates. From the different velocity maps described above, time series of reference MPs for each selected sector of the landslide body

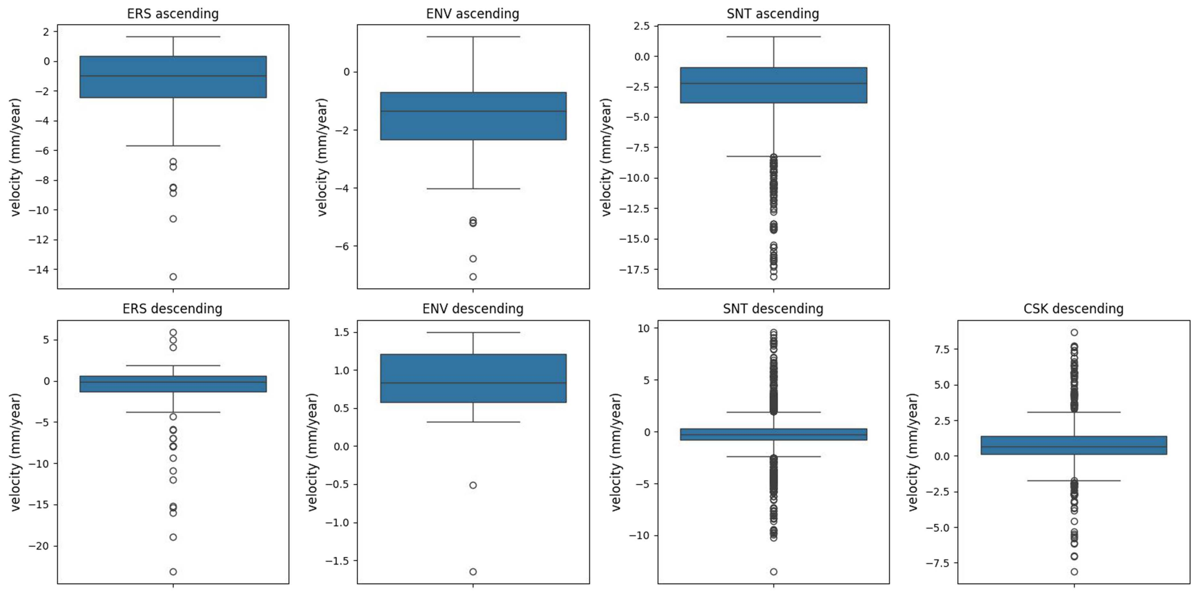

Figure 8. Boxplots showing the distribution of LoS displacement velocities obtained from ERS, ENV, SNT and CSK datasets for the entire landslide body in ascending (upper row) and descending (lower row) acquisition geometries.

over the period of 1992–2021 were extracted. The cumulative displacement time series for each sector in both the ascending and the descending orbit is presented in Figure 9.

Data along both the ascending and the descending orbit have mainly noiseless time series. Regarding the absolute displacement values, the ascending orbit time series show higher cumulative displacement values than the descending ones (with a difference of more than 100 mm over 30 years). The eastern slope section of the Mendatica village (i.e. LS2) recorded the highest displacement values among the three sectors for the entire period of analysis, with a total cumulated displacement of 269.5 and 160.8 mm along the ascending and descending orbit, respectively. The lowest values of displacement were recorded at the LS3 sector, with a total displacement, after 30 years, of 28.8 and 7.0 mm in the ascending and descending orbit, respectively. The slope portion encompassing LS1 shows intermediate values of total displacement, namely, 149.1 and 42.6 mm in the ascending and descending orbit, respectively. Several changes in the displacement trend can be noticed, principally affecting LS2, with acceleration and deceleration phases, especially in the ascending orbit data (highlighted in Figure 9a with red circles), which often seem related to rainfall conditions. For instance, in 1998, after an acceleration period, a deceleration phase began. Other bending points in cumulative displacements trends are visible in 2003 (acceleration to deceleration) and in 2007 (new acceleration phase). Interestingly, in the period of 2007–2010, satellite data appear highly consistent with geotechnical monitoring (see Figure 6), proving a particularly intense activity of the sector. From 2015 to 2021 a constant deformation trend is visible, and no significant acceleration phases are detected in any sector of the landslide.

Comparison between InSAR and inclinometer data

In this section, the comparison between InSAR data and inclinometric measurements is presented (Figure 10).

The S5–S15 inclinometric pair and the S1 tube have been considered since they were positioned within the most representative sectors (i.e. LS2 and LS1) of landslide evolution during the analysed period (see Figures 6 and 7). The selected inclinometers showed sharp and well-defined major sliding surfaces (see Figures 4 and 5). This allowed assuming that above the main levels of concentrated deformation, the cumulative deep displacement moduli are constant with depth. Moreover, the inclinometric displacements showed very similar azimuthal directions that can be assumed to be roughly parallel to the satellite LOS (compare Figures 6 and 7). Under these hypotheses, the subsurface horizontal displacements from the

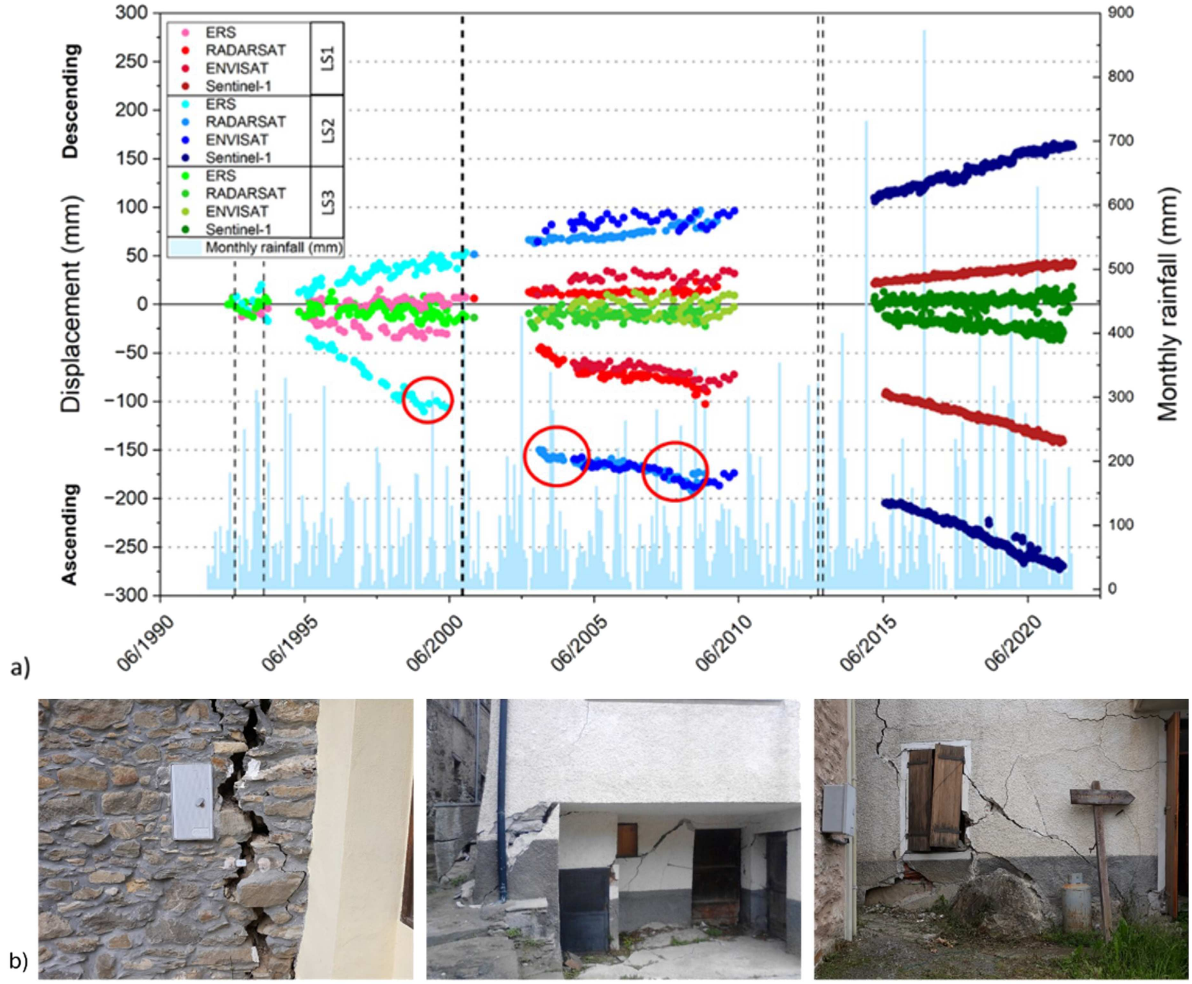

Figure 9. (a) Ascending and descending displacement time series (period 1992–2021) for the three selected sectors of the Mendatica landslide. The red circles highlight bending points in the time series, representing trend changes (acceleration to deceleration and vice versa). The dashed lines represent the most important evidence of damaging events known from historical information (occurred on 1 January 1993, 1 January 1994, 6 November 2000, 23 November 2000, 1 March 2013 and 1 May 2013). (b) Damage to buildings and infrastructures occurred in 2013.

inclinometers were assumed to be reasonably comparable with the surface displacements from InSAR data. The descending CSK dataset was also considered since X-band satellite products have finer spatial resolution than C-band satellites (Figure 10). Thus, satellite LoS displacements for both ascending and descending orbits were compared with cumulative incremental subsurface displacements obtained from inclinometers.

As previously noted in Figure 8, the ascending orbit data showed higher total displacements than the descending ones, leading to more pronounced acceleration trends. At a first glance, the correlation between the satellite and inclinometer monitoring data reveals coherent movement patterns (Figure 10b and c). Notably, SNT data acquired in descending geometry show nearly perfect alignment with ground-based measurements from tube S15, closely matching acceleration/deceleration trends and displacement values (Figure 10b), due to the slope orientation being aligned with the satellite LoS in the descending geometry. The comparison between the cumulative local horizontal displacements measured in tubes S5–S15 and the interferometric LoS displacement data of MPs, in ascending and descending orbits, reveals two main similar trends (Figure 10b). In the former, subsurface displacements recorded by tube S5 indicate a strong acceleration phase beginning in late 2007 and causing casing disruption in late 2009, which is consistent with the RST dataset in both acquisition geometries. In the latter, comparing ground-based data with the SNT dataset shows alternating acceleration and deceleration phases (e.g. increasing trend from

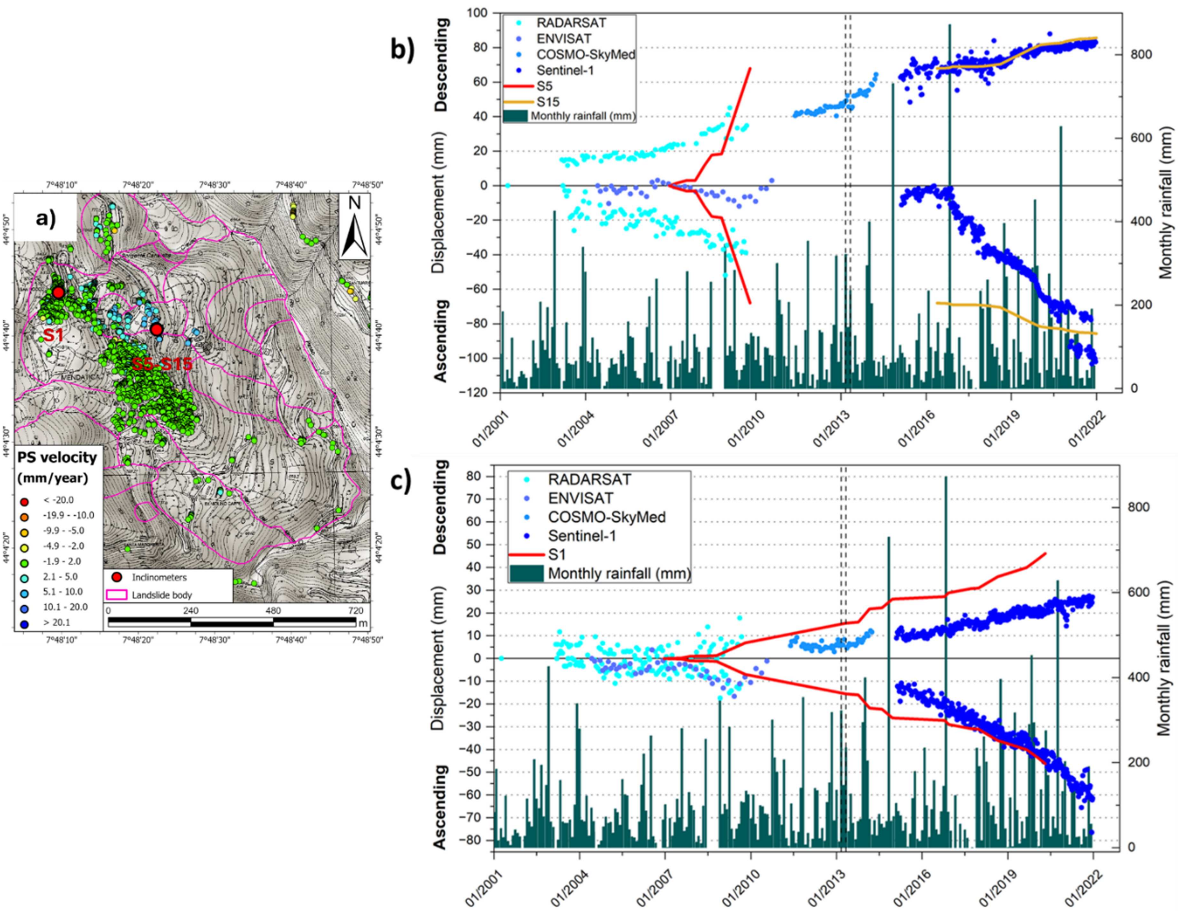

Figure 10. (a) Velocity map of MPs located within the investigated portion of the Mendatica landslide obtained from the CSK dataset in descending orbit and used for the comparison with inclinometric data together with the other InSAR datasets. (b and c) Comparison between displacement time series from inclinometer measures (cumulative incremental displacements referred to the resultant of movement in tubes S5–S15 and S1) and InSAR data (ascending and descending orbits). The black dashed lines indicate the main reactivation/acceleration phases (occurred in March and May 2013).

August 2018 to January 2020). Moreover, interesting outcomes emerge from the CSK time series, indicating strong acceleration in 2013 (more than 20 mm in one year), which is coincident with the last major damaging event (see Figure 9b). Unfortunately, this important acceleration was not detected by *in situ* equipment, as there were no active tubes in this sector. Likewise, comparing interferometric LoS displacement with measurements from tube S1 reveals similar patterns of displacement (Figure 10c). The acceleration detected by the CSK dataset in 2013 aligns temporally with the increasing trend measured by the inclinometer. Another increasing motion trend detected by inclinometer S1, starting around September 2017, matches quite well with that of the SNT dataset in timing and displacement magnitude.

By analyzing the relations between monthly rainfall and InSAR MP time series, a significant acceleration from November 2016 to June 2018 is clearly visible, especially in the ascending orbit data, following substantial rainfall (873 mm). This anomalous trend was not fully detected by inclinometer data both from tubes S5–S15 and S1. Another acceleration was recorded by inclinometer S1 from October 2020 to October 2021, again after a high amount of rainfall (628 mm).

Kinematic model reconstruction

Based on the outcomes presented in the previous sections, displacement data retrieved from inclinometers and InSAR have been qualitatively examined in conjunction with geomorphological interpretation to outline the main characteristics of the displacement mechanisms affecting the northern and eastern zones of the Mendatica slope. Two longitudinal engineering-geological cross-sections aimed at describing the landslide structure along with its kinematic model have been reconstructed. The cross-sections have been roughly oriented parallel to the slope dip direction (see Figures 6 and 11) and to the average azimuth of movement vectors determined from inclinometer measurements (see Figure 6). Since the slope faces eastward, it is possible to assume the highest displacement values along the East-West component and the absence of N–S deformation components. Thus, the vertical and horizontal (E–W) deformation components retrieved from RST and SNT constellations were employed (Figure 11). These two SAR datasets showed the highest MP density and cover periods characterized by the most significant spatial and temporal frequency of geotechnical monitoring (see Figure 3). In this regard, the mean yearly velocities of subsurface horizontal displacements recorded by inclinometers over the periods covered by RST (i.e. 2006/2009) and SNT data (i.e. 2017–2021) have been considered (Figure 11). To reconstruct the landslide kinematic model, the inclinometers closest to the traces of the cross-sections were considered, while MPs located within a 15-m buffer zone around each trace were extracted. In addition, the inclinometric profiles were also examined to delineate the location and geometry of the presumed failure surfaces (Figure 12).

The spatial distribution of MPs along the two selected slope sections reveals that the horizontal components of movement are predominant (Figure 11). In the northern and eastern zones of the slope, clusters of MPs showed positive velocities ranging between 2.1 and 10 mm/yr in the RST dataset and between 2.1 and 20 mm/yr in the SNT dataset, both indicating eastward movements. Conversely, the vertical displacements were constantly lower and in the order of no more than 5 mm/year in both SAR datasets, albeit some isolated SNT MPs reached downward velocities of around 10 mm/yr. This finding is consistent with ground-based monitoring data, as the inclinometers showing the highest mean horizontal velocities are in the same slope sectors (Figure 11), especially in the RST period.

Both InSAR results and *in situ* monitoring indicate that the downslope movements are consistently directed towards the path of the Passo Cagnasso stream (compare Figures 6 and 11), suggesting that the erosion of the landslide toe operated by this stream may represent a driving factor of instability. This is also testified by the abrupt variation in steepness at the lowermost part of the slope (average slope gradient of 30°) with respect to the upslope sections (average slope gradient of 20°) (Figure 12). It is worth noting that the spatial correspondence between InSAR and inclinometer measurements is less evident at the slope foot due to the limited number of available MPs. However, based on the similar morphological setting and the comparable magnitude of subsurface displacements measured by inclinometers, a similar pattern of movement can be reasonably assumed across this part of the unstable slope. Indeed, similar to upslope sections, the foot sector is affected by several zones of depletion along with smoothed scarps connected to secondary landslide bodies (Figure 11).

Discussion

The Mendatica landslide presents a long and complex history of instability phases, which was the source of widespread and severe damage to the built asset. In previous studies, to shed light on complex landslide kinematic behaviour, neither the exclusive employment of ground-based monitoring techniques nor the use of remotely sensed data was not enough (Notti, Herrera et al., 2014; Cevasco and Pepe, 2016; Pepe et al., 2021). In this work, the combined use of both approaches attempted to reconstruct the deformation history over almost 30 years along with characterising the geometric and kinematic features of the most unstable urbanized portion of the landslide. Specifically, the concurrent measurement of ground surface displacements by InSAR and of subsurface movements with *in situ* monitoring equipment over more than 15 years played a very important role.

The use of InSAR technique implies the compromise of measuring only the component of the movement parallel to the satellite LoS, leading to a possible underestimation of the actual displacement rate based on the slope geometry (Wasowski & Bovenga, 2014), while slope inclinometers are suitable for measuring very small displacements rates that do not depend on slope orientation (Wasowski & Pisano, 2020). In the case of the Mendatica landslide, the orientation of the slope, facing east and nearly parallel to the satellite LoS, allowed a satisfactory estimation of ground movements. Basically, from the early 1990s to 2021, the mean LoS displacement rates detected from InSAR for both acquisition geometries indicated an almost regular spatial pattern of landslide activity (Figure 7). Moreover, the InSAR outcomes were well

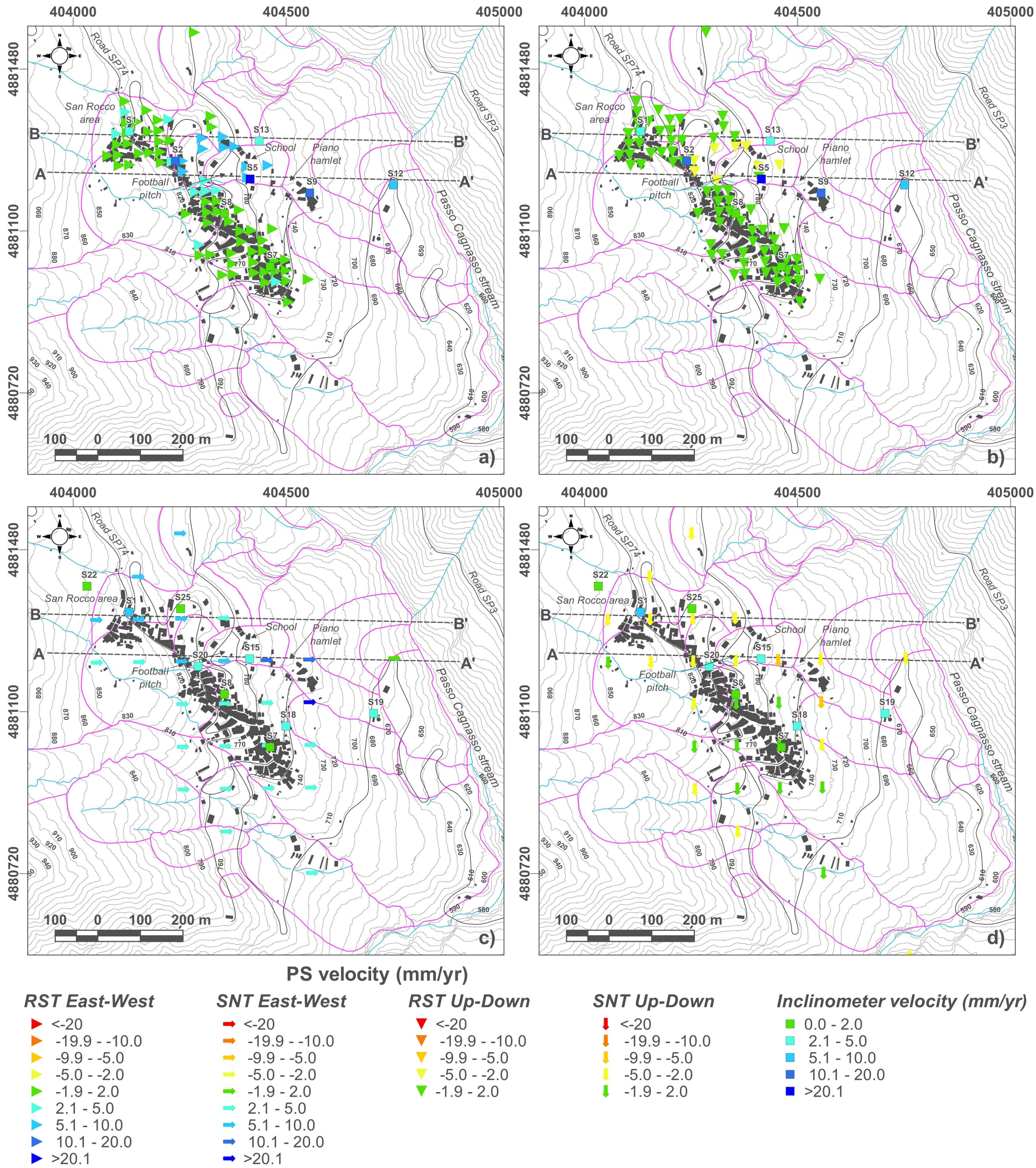

Figure 11. PS velocity maps of RST horizontal (E–W) (a) and vertical (b) components and of SNT horizontal (E–W) (c) and vertical (d) components. Square symbols indicate the location of the inclinometers and are coloured based on the mean velocity measured in the period of each satellite dataset. The black dashed lines indicate the traces of longitudinal cross sections shown in Figure 12.

consistent for all the satellite datasets considered. The portion of the landslide body characterized by substantially stable conditions coincided with the southern and western parts of the Mendatica village, where the MP motion was almost always within the stable range (±2 mm/yr) (Figure 7). Similarly, the inclinometer tubes did not register significant movements, denoted by mean rates of displacement lower than 3 mm/yr over almost 10-year monitoring periods (Figures 6 and 11). Conversely, the middle-upper portions of the landslide affecting the eastern and northern urban area were regularly unstable (Figure 7). The most moveable radar targets presented mean rates normally ranging between 5 and 20 mm/yr, corresponding to extremely to very slow movements (Cruden and Varnes, 1996). In agreement with

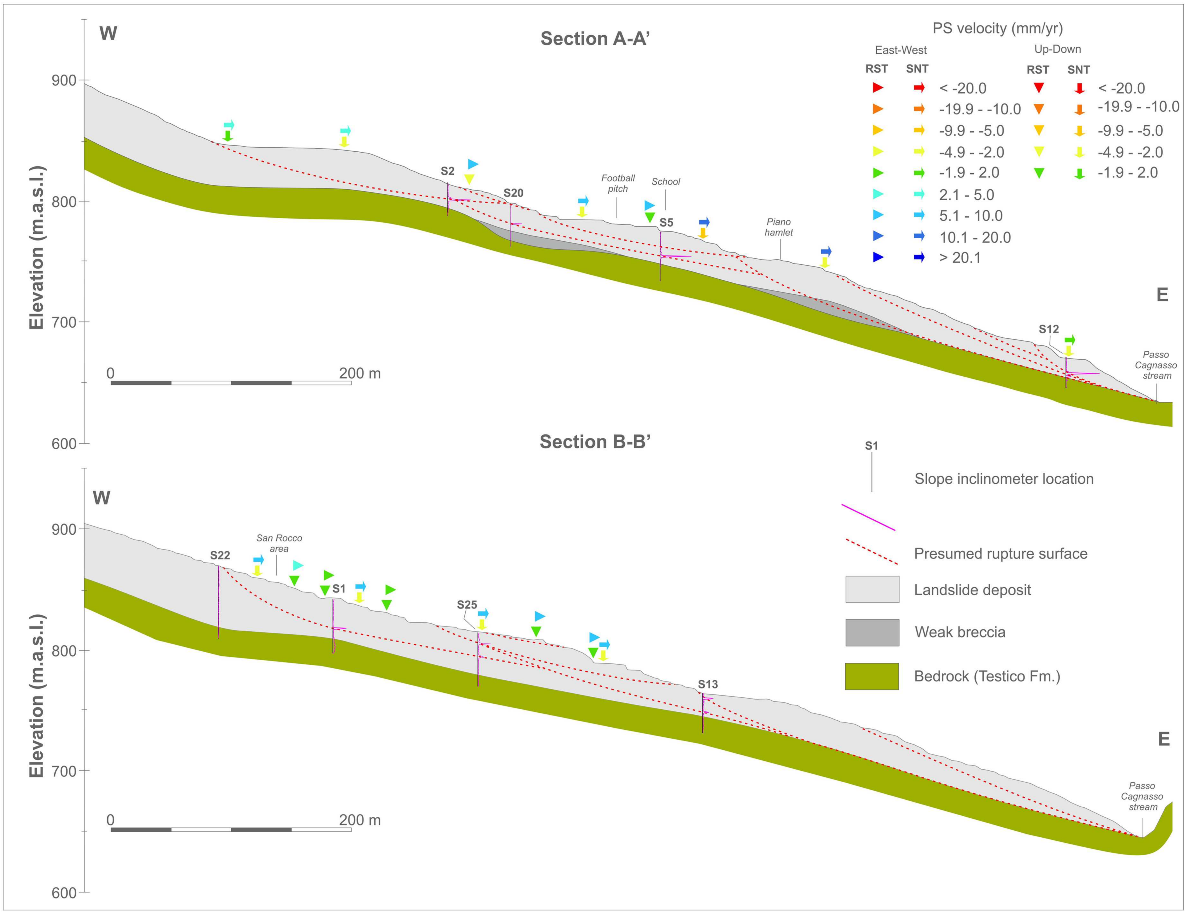

Figure 12. Longitudinal engineering–geological cross sections employed for defining the kinematic model of the active portions of the Mendatica landslide are based on the interpretation of inclinometer and InSAR data together with geomorphological evidence. MPs located within 15-m buffer zones around the trace of each cross-section are reported with different symbols and colour according to the satellite dataset, the average yearly velocity and the deformation component (i.e. vertical and horizontal).

InSAR data, the measurement of subsurface displacements along the inclinometers indicated these zones as the most active ones (Figures 6 and 11), which is further supported by the shearing of some casing tubes, and by the most severe levels of damage suffered from buildings and infrastructures (Federici et al., 2007; Pepe et al., 2021). In these sectors, the displacement time series of inclinometers were found to be adequately comparable to those of InSAR in terms of order of magnitude, whereas they closely matched in terms of trends since both monitoring datasets were able to capture the main movement patterns (Figure 10). Notably, from 2015 onwards, the last available satellite dataset (i.e. SNT) revealed clues of retrogressive evolution of the landslide activity in the uppermost area of the village (i.e. San Rocco hamlet). This was also testified by the slight increase in the deformation rate detected by the inclinometer S1, which was installed in this area (Figures 6 and 11). Therefore, this evidence highlights that the greater spatial completeness of the SNT dataset can have high potential in achieving a dynamic zonation of landslide activity in case of large, deep-seated and extremely slow-moving landslides affecting urban centres. On the other hand, the low density of MPs, due to the presence of highly vegetated areas and the absence of building and infrastructure clusters, limited the accurate definition of the spatial distribution of the state of activity at the landslide foot (Figure 7). Indeed, the low density of reflectors may lead to an underestimation of the displacement rate distribution since areas with higher velocity may be covered by vegetation, making them undetectable using the interferometric technique. Further sources of uncertainty include atmospheric phase delays, temporal and geometrical decorrelation and residual orbital inaccuracies, all of which can bias the retrieved LoS velocities (Crosetto et al., 2016). The accuracy of PS velocity estimation after atmospheric phase screen removal can be lower than 1 mm/yr, depending on the number of SAR acquisitions, PS density and temporal baseline dispersion (Colesanti et al., 2003). In this study, considering the data quality and coherence distribution, uncertainties of a few millimetres per year are expected, particularly in vegetated or decorrelated areas. Upslope from the landslide foot sector, the available inclinometers exhibited active movements, with intensities comparable with those detected by satellites, as testified by the shearing of tubes S9 and S12 (Figure 6). Furthermore, thanks to the availability of the CSK dataset, it was possible to capture the occurrence of the most recent and important acceleration of the landslide (Figure 10), which was not detected by inclinometers, as they were irreparably damaged in that period, thus limiting the accurate investigation of subsurface movements. Nevertheless, the study outcomes highlighted as the combination of InSAR and ground-based monitoring data allows to successfully balance the limitations of each technique (Peduto et al., 2021; Refice et al., 2019; Wasowski & Pisano, 2020). On the one hand, SAR interferometry proves effective in overcoming drawbacks of geotechnical tools due to equipment maintenance, allowing us to decipher the temporal evolution of slow landslides. On the other hand, slope inclinometers can provide useful information when no significant radar benchmarks are detectable.

By qualitatively combining horizontal (East–West) and vertical components from InSAR data with horizontal displacements measured by inclinometers along the maximum slope direction, it has been possible to highlight somewhat regular spatial patterns of movement, mainly consisting of predominant eastward horizontal components associated with slight vertical deformations (Figure 11). This joint analysis supports the interpretation of composite styles of movement (WP/WLI, 1993). The several parts of the unstable slope seem to slide downslope through a combination of predominant translational movements coupled with weak rotational mechanisms. Inclinometric data concur to corroborate this style of movement since subsurface horizontal displacement profiles pointed out that the landslide mass generally moves along well-defined multiple failure surfaces with limited internal deformation (Figure 12).

Both monitoring datasets indicated that the landslide experienced almost continuous movements consisting of the alternation of acceleration and deceleration trends, with the most marked accelerations recorded in the period 2006–2013. For this period, the relations between the displacement and rainfall data was complex and no straightforward connections were found. Despite more severe rainfall conditions, the recent monitoring data series (period 2015–2021) apparently revealed a decrease in the frequency of sharp acceleration episodes. The highest rainfall levels were produced by severe and short-duration rainstorms, never recorded before. This fact would suggest that single and intense rain impulses can have a minor role on the landslide mobility. However, it is recognized that the mobility of deep-seated landslides can be controlled by several conditions beyond rainfall (e.g. Lacroix et al. (2020) and reference therein). Also, for the studied landslide, other factors should be considered, such as the subsurface hydrogeological setting and groundwater circulation (Passalacqua et al., 2016; Pepe et al., 2021). In this regard, it should be emphasized that the stabilization interventions installed over time may have modified the groundwater regime and consequently the landslide kinematic behaviour. Furthermore, the outcomes of geotechnical and InSAR investigations consistently indicated that the average directions of movement remained steadily oriented towards the path of the stream that flows at the slope toe. In light of this, it may be reasonably supposed that the movement dynamics also depend on the erosion of the landslide toe. This finding corroborates previous hypotheses based on geomorphological evidence on the factors controlling landslide behaviour (Federici et al., 2007). As reported in the literature, the geomorphological dynamics affecting the landslide toe can have relevant influences on the mobility of slow-moving landslides (Delchiaro et al., 2024, Ferrari et al., 2011). Because of foot failure, landslide masses can sometimes accelerate rapidly and catastrophically, as occurred in other large ancient landslides near the study area (Notti et al., 2021).

Conclusions

In this work, a joint application of remotely sensed and ground-based data has been adopted to monitor and investigate residual activity involving the urbanized sectors of the Mendatica relict landslide. Thanks to the complementary nature of InSAR technique and slope inclinometers, it was possible to reconstruct the landslide patterns of movement from both temporal and a spatial point of view, along with to qualitatively interpret the style and typology of the movement mechanisms. InSAR data from different constellations (i.e. ERS, RST, ENVISAT, CSK and SNT) over a period of more than 30 years and *in situ* measurements covering 15 years were used. In areas characterized by the longest displacement time series, *in situ* and InSAR monitoring results were cross compared to analyse their degree of correspondence.

The obtained outcomes revealed that both datasets provided coherent results concerning the spatial distribution of landslide activity, allowing to constrain the zones of the urban area affected by the most relevant intensities of movement. Moreover, the comparison between displacements measured from InSAR targets and those from nearby inclinometers showed that both monitoring techniques were able to capture the main movement patterns observed over the monitoring period, often characterized by alternating acceleration and deceleration trends. The use of InSAR datasets at higher resolution (i.e. CSK and SNT), owing to the higher density of targets as well as their more accurate location, concurred to achieve a more detailed investigation of the spatial–temporal evolution of deformation affecting some urbanized sectors. On the other hand, in the peripheral areas of the village, where the number of radar benchmarks can be very low, the availability of inclinometers, provided that they are adequately maintained, was crucial to avoid a lack of information. The integrated use of vertical and horizontal (E–W) displacement components from InSAR and subsurface horizontal displacements from inclinometers, together with the support of geomorphological evidence, proved effective in reconstructing the kinematic model and the subsurface structure of the moving sectors and thus in interpreting the movement types and styles.

This study provided useful insights on the coupled analysis of InSAR and geotechnical multitemporal data series for monitoring slow-moving urbanized landslides as well as improving the level of knowledge on their kinematics with reference to the slope scale and to a medium-to-long temporal window. The analysis highlighted the advantages deriving from the use of InSAR data acquired through favourable satellite viewing geometry. Moreover, in such situations, it should be emphasized that the design of *in situ* monitoring networks and their maintenance over time remain essential. The outcomes of this study may represent a helpful knowledge basis for future studies devoted to model factors controlling the movement patterns of the Mendatica landslide, especially those driving scenarios of more severe reactivations. Finally, the virtuous use of spaceborne and ground-based monitoring of relict urbanized landslides can have useful implications for practical applications in landslide management or urban planning, such as the zonation of landslide activity and intensity along with the design of effective remedial works aimed at mitigating hazard and risk.

Acknowledgements

This study was carried out within the RETURN Extended Partnership and received funding from the European Union Next-GenerationEU (National Recovery and Resilience Plan – NRRP, 816 Mission 4, Component 2, Investment 1.3 – D.D. 1243 2/8/2022, PE0000005).

Author contributions

Francesco Barbadori: methodology, formal analysis, writing – original draft. Saduni Melissa Dahanayaka: methodology, formal analysis, writing – original draft. Matteo Del Soldato: conceptualization, methodology, writing – review and editing, supervision. Fabio Arrighetti: resources, investigation. Tommaso Macciò: resources, investigation. Roberto Macciò: resources, investigation. Andrea Cevasco: resources, writing – review and editing, supervision. Giacomo Pepe: conceptualization, methodology, writing – original draft, supervision.

Disclosure statement

No potential conflict of interest was reported by the author(s).

ORCID

Francesco Barbadori 0000-0001-6573-3721
Saduni Melissa Dahanayaka 0009-0008-2740-9435
Matteo Del Soldato 0000-0001-7539-5850
Andrea Cevasco 0000-0002-0559-4835
Giacomo Pepe 0000-0002-5435-6462

Data availability statement

The data that support the findings of this study are openly available in Mendeley at https://data.mendeley.com/datasets/3k8t43xs2x/1.

References

Attema, E., Duchossois, G., & Kohlhammer, G. (1998). ERS-1/2 SAR land applications: Overview and main results. In IGARSS'98 Organizing Committee (Ed.), *Sensing and Managing the Environment. 1998 IEEE International Geoscience and Remote Sensing. TNFPP_CopyEditCatCProceedings* (Cat. No. 98CH36174). IEEE.

Berardino, P., Fornaro, G., Lanari, R., & Sansosti, E. (2002). A new algorithm for surface deformation monitoring based on small baseline differential SAR interferograms. *IEEE Transactions on Geoscience and Remote Sensing*, *40*(11), 2375–2383. https://doi.org/10.1109/TGRS.2002.803792

Blanco-Sanchez, P., Mallorquí, J. J., Duque, S., & Monells, D. (2008). The coherent pixels technique (CPT): An advanced DInSAR technique for nonlinear deformation monitoring. *Pure and Applied Geophysics*, *165*(6), 1167–1193. https://doi.org/10.1007/s00024-008-0352-6

Bordoni, M., Vivaldi, V., Bonì, R., Spanò, S., Tararbra, M., Lanteri, L., Parnigoni, M., Grossi, A., Figini, S., & Meisina, C. (2023). A methodology for the analysis of continuous time-series of automatic inclinometers for slow-moving landslides monitoring in Piemonte region, northern Italy. *Natural Hazards*, *115*(2), 1115–1142. https://doi.org/10.1007/s11069-022-05586-3

Bru, G., Ezquerro, P., Azañón, J. M., Mateos, R. M., Tsige, M., Béjar-Pizarro, M., & Guardiola-Albert, C. (2024). Deceleration captured by InSAR after local stabilization works in a slow-moving landslide: The case of Arcos de la Frontera (SW Spain). *Landslides*, *21*, 1–17. https://doi.org/10.1007/s10346-024-02292-y

Bruzzi, S., Louet, J., & Pfeiffer, B. (1995). ENVISAT-1 system and mission. *Space Technology*, *3*(15), 145–155. https://doi.org/10.1016/0892-9270(95)00024-Y

Calò, F., Ardizzone, F., Castaldo, R., Lollino, P., Tizzani, P., Guzzetti, F., Lanari, R., Angeli, M.-G., Pontoni, F., & Manunta, M. (2014). Enhanced landslide investigations through advanced DInSAR techniques: The Ivancich case study, Assisi, Italy. *Remote Sensing of Environment*, *142*, 69–82. https://doi.org/10.1016/j.rse.2013.11.003

Calò, F., Calcaterra, D., Iodice, A., Parise, M., & Ramondini, M. (2012). Assessing the activity of a large landslide in southern Italy by ground-monitoring and SAR interferometric techniques. *International Journal of Remote Sensing*, *33*(11), 3512–3530. https://doi.org/10.1080/01431161.2011.630331

Capes, R., & Passera, E. (2022). *End-to-end implementation and operation of the European Ground Motion Service (EGMS). Product description and format specification*. European Ground Motion Service.

Cenni, N., Fiaschi, S., & Fabris, M. (2021). Integrated use of archival aerial photogrammetry, GNSS, and InSAR data for the monitoring of the Patigno landslide (Northern Apennines, Italy). *Landslides*, *18*(6), 2247-2263.10.1007/s10346-021-01635-3

Cevasco, A., Pepe, G., Macciò, R., Arrighetti, F., De Stefanis, E., Poggi, F., Boni, R., & Firpo, M. (2016). Interactions between relict landslides and built environment: Hazard investigations and monitoring at Mendatica (Western Liguria, Italy). *Rendiconti Online della Società Geologica Italiana*, *40*(Suppl. 1), 668–668.

Cevasco, A., Termini, F., Valentino, R., Meisina, C., Bonì, R., Bordoni, M., Chella, G., & De Vita, P. (2018). Residual mechanisms and kinematics of the relict Lemeglio coastal landslide (Liguria, northwestern Italy). *Geomorphology*, *320*, 64–81. https://doi.org/10.1016/j.geomorph.2018.08.010

Colesanti, C., Ferretti, A., Prati, C., & Rocca, F. (2003). Monitoring landslides and tectonic motions with the permanent scatterers technique. *Engineering Geology*, *68*(1), 3–14. https://doi.org/10.1016/S0013-7952(02)00195-3

Confuorto, P., Casagli, N., Casu, F., De Luca, C., Del Soldato, M., Festa, D., Lanari, R., Manzo, M., Onorato, G., & Raspini, F. (2023). Sentinel-1 P-SBAS data for the update of the state of activity of national landslide inventory maps. *Landslides*, *20*(5), 1083-1097. https://doi.org/10.1007/s10346-022-02024-0

Confuorto, P., Di Martire, D., Infante, D., Novellino, A., Papa, R., Calcaterra, D., & Ramondini, M. (2019). Monitoring of remedial works performance on landslide-affected areas through ground-and satellite-based techniques. *Catena*, *178*, 77–89. https://doi.org/10.1016/j.catena.2019.03.005

Costantini, M., Falco, S., Malvarosa, F., & Minati, F. (2008). A new method for identification and analysis of persistent scatterers in series of SAR images. In IEEE Geoscience and Remote Sensing Society (Ed.), *IGARSS 2008 International Geoscience and Remote Sensing Symposium* (pp. II-449–II-452). IEEE. https://doi.org/10.1109/IGARSS.2008.4779025

Costantini, M., Falco, S., Malvarosa, F., Minati, F., & Trillo, F. (2009). Method of persistent scatterer pairs (PSP) and high resolution SAR interferometry. In IEEE Geoscience and Remote Sensing Society (Ed.), *2009 IEEE International Geoscience and Remote Sensing Symposium* (Vol. 3, pp. II–904). IEEE.

Costantini, M., Falco, S., Malvarosa, F., Minati, F., Trillo, F., & Vecchioli, F. (2014). Persistent scatterer pair interferometry: Approach and application to COSMO-SkyMed SAR data. *IEEE Journal of Selected Topics in Applied Earth Observations and Remote Sensing*, *7*(7), 2869–2879. https://doi.org/10.1109/JSTARS.2014.2343915

Costantini, M., Ferretti, A., Minati, F., Falco, S., Trillo, F., Colombo, D., Novali, F., Malvarosa, F., Mammone, C., & Vecchioli, F. (2017). Analysis of surface deformations over the whole Italian territory by interferometric processing of ERS, Envisat and COSMO-SkyMed radar data. *Remote Sensing of Environment*, *202*, 250–275. https://doi.org/10.1016/j.rse.2017.07.017

Costantini, M., Minati, F., Trillo, F., Ferretti, A., Novali, F., Passera, E., Andersen, H. S., Dehls, J., Larsen, Y., Marinkovic, P., Eineder, M., Brcic, R., Siegmund, R., Kotzerke, P., Probeck, M., Kenyeres, A., Proietti, S., & Solari, L. (2021). European ground motion service (EGMS). In IEEE Geoscience and Remote Sensing Society (Ed.), *2021 IEEE International Geoscience and Remote Sensing Symposium IGARSS* (pp. 3293–3296). IEEE. https://doi.org/10.1109/IGARSS47720.2021.9553562

Crosetto, M., Monserrat, O., Cuevas-González, M., Devanthéry, N., & Crippa, B. (2016). Persistent scatterer interferometry: A review. *ISPRS Journal of Photogrammetry and Remote Sensing*, *115*, 78–89. https://doi.org/10.1016/j.isprsjprs.2015.10.011

Crosetto, M., Solari, L., Mróz, M., Balasis-Levinsen, J., Casagli, N., Frei, M., Oyen, A., Moldestad, A., Bateson, L., & Guerrieri, L. (2020). The evolution of wide-area DInSAR: From regional and national services to the European ground motion service. *Remote Sensing*, *12*(12), 2043.

Decarlis, A., Dallagiovanna, G., Lualdi, A., Maino, M., & Seno, S. (2013). Stratigraphic evolution in the Ligurian Alps between Variscan heritages and the Alpine Tethys opening: A review. *Earth-Science Reviews*, *125*, 43-68.10.1016/j.earscirev.2013.07.001

Delchiaro, M., Della Seta, M., Martino, S., Moumeni, M., Nozaem, R., Marmoni, G. M., & Esposito, C. (2024). The role of long-term preparatory factors in mass rock creep deforming slopes: Insights from the Zagros Mts. belt (Iran). *Landslides*, 21(8), 1735–1755. https://doi.org/10.1007/s10346-024-02252-6

Del Soldato, M., Riquelme, A., Bianchini, S., Tomàs, R., Di Martire, D., De Vita, P., Moretti, S., & Calcaterra, D. (2018). Multisource data integration to investigate one century of evolution for the Agnone landslide (Molise, southern Italy). *Landslides*, 15(11), 2113–2128.

Di Maio, C., Fornaro, G., Gioia, D., Reale, D., Schiattarella, M., & Vassallo, R. (2018). *In situ* and satellite long-term monitoring of the Latronico landslide, Italy: Displacement evolution, damage to buildings, and effectiveness of remedial works. *Engineering Geology*, *245*, 218–235. https://doi.org/10.1016/j.enggeo.2018.08.017

Duro, J., Inglada, J., Closa, J., Adam, N., & Arnaud, A. (2004). High resolution differential interferometry using time series of ERS and ENVISAT SAR data. In European Space Agency (Ed.), *FRINGE 2003 Workshop: Space radar advances and applications* (pp. 1–5). European Space Agency.

Eineder, M. (2003). Efficient simulation of SAR interferograms of large areas and of rugged terrain. *IEEE Transactions on Geoscience and Remote Sensing*, *41*(6), 1415–1427. https://doi.org/10.1109/TGRS.2003.811692

Federici, P. R., Capitani, M., Chelli, A., Del Seppia, N., & Serani, A. (2007). Atlante dei Centri Abitati Instabili della Liguria. Provincia di Imperia. (Vol. IV). Genova: Tipografia Nuova Ata.

Ferretti, A., Fumagalli, A., Novali, F., Prati, C., Rocca, F., & Rucci, A. (2011). A new algorithm for processing interferometric data-stacks: SqueeSAR. *IEEE Transactions on Geoscience and Remote Sensing*, *49*(9), 3460–3470.

Ferrari, A., Ledesma, A., González, D., & Corominas, J. (2011). Effects of the foot evolution on the behaviour of slow-moving landslides. *Engineering Geology*, *117*(3–4), 217–228. https://doi.org/10.1016/j.enggeo.2010.11.001

Ferretti, A., Prati, C., & Rocca, F. (2001). Permanent scatterers in SAR interferometry. *IEEE Transactions on Geoscience and Remote Sensing*, *39*(1), 8–20. https://doi.org/10.1109/36.898661

Festa, D., & Del Soldato, M. (2023). EGMStream, a desktop app for EGMS data downstream. *Remote Sensing*, *15*(10), 2581. https://doi.org/10.3390/rs15102581

Geudtner, D., Torres, R., Snoeij, P., Davidson, M., & Rommen, B. (2014). Sentinel-1 System capabilities and applications. In IEEE Geoscience and Remote Sensing Society (Ed.), *Proceedings of the 2014 IEEE International Geoscience and Remote Sensing Symposium (IGARSS 2014)* (pp. 1457–1460). IEEE.

Giammarino, S., Fanucci, F., Anfossi, R., Arbarelli, C., Cobianchi, M., Cuppari, A., Dabove, G., De Stefanis, A., De Stefanis, P., & Stefano, A. (2010). *Carta Geologica d'Italia alla scala 1: 50.000-Foglio "San Remo" N. 258-271 con Note Illustrative*. ISPRA-Regione Liguria. ATI-SystemCart srl-LAC srl-S. EL. CA.

Hervás, J., Barredo, J. I., Rosin, P. L., Pasuto, A., Mantovani, F., & Silvano, S. (2003). Monitoring landslides from optical remotely sensed imagery: The case history of Tessina landslide, Italy. *Geomorphology*, *54*(1), 63–75. https://doi.org/10.1016/S0169-555X(03)00056-4

Iadanza, C., Trigila, A., Starace, P., Dragoni, A., Biondo, T., & Roccisano, M. (2021). IdroGEO: A collaborative web mapping application based on REST API services and open data on landslides and floods in Italy. *ISPRS International Journal of Geo-Information*, *10*(2), 89. https://doi.org/10.3390/ijgi10020089

Iglesias, R., Monells, D., López-Martínez, C., Mallorqui, J. J., Fabregas, X., & Aguasca, A. (2015). Polarimetric optimization of temporal sublook coherence for DInSAR applications. *IEEE Geoscience and Remote Sensing Letters*, *12*(1), 87–91. https://doi.org/10.1109/LGRS.2014.2326684

Jiaxuan, H., Mowen, X., & Atkinson, P. (2020). Dynamic susceptibility mapping of slow-moving landslides using PSInSAR. *International Journal of Remote Sensing*, *41*(19), 7509–7529. https://doi.org/10.1080/01431161.2020.1760398

Journault, J., Macciotta, R., Hendry, M. T., Charbonneau, F., Huntley, D., & Bobrowsky, P. T. (2018). Measuring displacements of the Thompson River valley landslides, south of Ashcroft, BC, Canada, using satellite InSAR. *Landslides*, *15*(4), 621–636. https://doi.org/10.1007/s10346-017-0900-1

Kjekstad, O., & Highland, L. (2009). Economic and social impacts of landslides. In K. Sassa, & P. Canuti (Eds.), *Landslides–disaster risk reduction* (pp. 573–587). Springer. https://doi.org/10.1007/978-3-540-69970-5_30

Lacroix, P., Handwerger, A. L., & Bièvre, G. (2020). Life and death of slow-moving landslides. *Nature Reviews Earth & Environment*, *1*(8), 404–419. https://doi.org/10.1038/s43017-020-0072-8
Lopez-Quiroz, P., Doin, M. P., Tupin, F., Briole, P., & Nicolas, J. M. (2009). Time series analysis of Mexico City subsidence constrained by radar interferometry. *Journal of Applied Geophysics*, *69*(1), 1–15. https://doi.org/10.1016/j.jappgeo.2009.02.006
Lopez Saez, J., Corona, C., Stoffel, M., Astrade, L., Berger, F., & Malet, J. P. (2012). Dendrogeomorphic reconstruction of past landslide reactivation with seasonal precision: The Bois Noir landslide, southeast French Alps. *Landslides*, *9*(2), 189–203. https://doi.org/10.1007/s10346-011-0284-6
Maino, M., & Seno, S. (2016). The thrust zone of the Ligurian Penninic basal contact (Monte Fronté, Ligurian Alps, Italy). *Journal of Maps*, *12*(Suppl. 1), 341–351. https://doi.org/10.1080/17445647.2016.1213669
Mather, A. E., Griffiths, J. S., & Stokes, M. (2003). Anatomy of a 'fossil' landslide from the Pleistocene of SE Spain. *Geomorphology*, *50*(1–3), 135–149. https://doi.org/10.1016/S0169-555X(02)00211-8
Meisina, C., Zucca, F., Notti, D., Colombo, A., Cucchi, A., Savio, G., Giannico, C., & Bianchi, M. (2008). Geological interpretation of PSInSAR data at regional scale. *Sensors*, *8*(11), 7469–7492. https://doi.org/10.3390/s8117469
Mikkelsen, P. E. (1996). Field instrumentation. In A. K. Turner, & R. L. Schuster (Eds.), *Landslides: Investigation and mitigation* (pp. 278–314). Transportation Research Board, National Research Council.
Mondini, A. C., Guzzetti, F., Chang, K.-T., Monserrat, O., Martha, T. R., & Manconi, A. (2021). Landslide failures detection and mapping using Synthetic Aperture Radar: Past, present and future. *Earth-Science Reviews*, 216, 103574.
Mora, O., Mallorqui, J. J., & Broquetas, A. (2003). Linear and nonlinear terrain deformation maps from a reduced set of interferometric SAR images. *IEEE Transactions on Geoscience and Remote Sensing*, *41*(10), 2243–2253. https://doi.org/10.1109/TGRS.2003.814657
Moretto, S., Bozzano, F., & Mazzanti, P. (2021). The role of satellite InSAR for landslide forecasting: Limitations and openings. *Remote Sensing*, *13*(18), 3735. https://doi.org/10.3390/rs13183735
Notti, D., Herrera, G., Bianchini, S., Meisina, C., García-Davalillo, J. C., & Zucca, F. (2014). A methodology for improving landslide PSI data analysis. *International Journal of Remote Sensing*, *35*(6), 2186-2214. https://doi.org/10.1080/01431161.2014.889864
Notti, D., Meisina, C., Zucca, F., Colombo, A., & Paro, L. (2014). Map and monitoring slow ground deformation in NW Italy using PSI techniques. In *Engineering geology for society and territory, vol 5: Urban geology, sustainable planning and landscape exploitation. 12th International IAEG Congress, Torino, Italy*.
Notti, D., Wrzesniak, A., Dematteis, N., Lollino, P., Fazio, N. L., Zucca, F., & Giordan, D. (2021). A multidisciplinary investigation of deep-seated landslide reactivation triggered by an extreme rainfall event: A case study of the Monesi di Mendatica landslide, Ligurian Alps. *Landslides*, *18*, 2341–2365.
Novellino, A., Pennington, C., Leeming, K., Taylor, S., Alvarez, I. G., McAllister, E., Arnhardt, C., & Winson, A. (2024). Mapping landslides from space: A review. *Landslides*, 21(5), 1041–1052.
Passalacqua, R., Bovolenta, R., Federici, B., & Balestrero, D. (2016). A physical model to assess landslide susceptibility on large areas: Recent developments and next improvements. *Procedia Engineering*, *158*, 487–492. https://doi.org/10.1016/j.proeng.2016.08.477
Peduto, D., Santoro, M., Aceto, L., Borrelli, L., & Gullà, G. (2021). Full integration of geomorphological, geotechnical, A-DInSAR and damage data for detailed geometric-kinematic features of a slow-moving landslide in urban area. *Landslides*, *18*, 807–825. https://doi.org/10.1007/s10346-020-01541-0
Pepe, G., Cevasco, A., Piazza, M., Macciò, R., Arrighetti, F., & Casagli, N. (2021). On the efficiency and effectiveness of automatic deep drainage systems during an extreme rainfall event: The Mendatica landslide case study (Western Liguria, Italy). *Landslides*, *18*(12), 3799–3820. https://doi.org/10.1007/s10346-021-01740-3
Prats-Iraola, P., Scheiber, R., Marotti, L., Wollstadt, S., & Reigber, A. (2012). TOPS interferometry with TerraSAR-X. *IEEE Transactions on Geoscience and Remote Sensing*, *50*(8), 3179–3188.
Raspini, F., Bianchini, S., Ciampalini, A., Del Soldato, M., Solari, L., Novali, F., Del Conte, S., Rucci, A., Ferretti, A., & Casagli, N. (2018). Continuous, semi-automatic monitoring of ground deformation using Sentinel-1 satellites. *Scientific Reports*, *8*, 7253. https://doi.org/10.1038/s41598-018-25369-w
Refice, A., Spalluto, L., Bovenga, F., Fiore, A., Miccoli, M., Muzzicato, P., Nitti, D., Nutricato, R., & Pasquariello, G. (2019). Integration of persistent scatterer interferometry and ground data for landslide monitoring: The Pianello landslide (Bovino, Southern Italy). *Landslides*, *16*, 447–468. https://doi.org/10.1007/s10346-018-01124-0
Rosi, A., Tofani, V., Tanteri, L., Tacconi Stefanelli, C., Agostini, A., Catani, F., & Casagli, N. (2018). The new landslide inventory of Tuscany (Italy) updated with PS-InSAR: Geomorphological features and landslide distribution. *Landslides*, *15*(1), 5–19. https://doi.org/10.1007/s10346-017-0861-4
Sansosti, E., Berardino, P., Manunta, M., Serafino, F., & Fornaro, G. (2006). Geometrical SAR image registration. *IEEE Transactions on Geoscience Remote Sensing*, *44*(10), 2861-2870.
Serva, S., Fiorentino, C., & Covello, F. (2015). The COSMO-SkyMed seconda generazione key improvements to respond to the user community needs. In IEEE Geoscience and Remote Sensing Society (Ed.), *2015 IEEE International Geoscience and Remote Sensing Symposium (IGARSS)*. IEEE.
Simeoni, L., & Mongiovì, L. (2007). Inclinometer monitoring of the Castelrotto landslide in Italy. *Journal of Geotechnical Geoenvironmental Engineering*, *133*(6), 653–666. https://doi.org/10.1061/(ASCE)1090-0241(2007)133:6(653)

Simeoni, L., Ronchetti, F., Costa, C., Joris, P., & Corsini, A. (2020). Redundancy and coherence of multi-method displacement monitoring data as key issues for the analysis of extremely slow landslides (Isarco valley, Eastern Alps, Italy). *Engineering Geology*, *267*, 105504. https://doi.org/10.1016/j.enggeo.2020.105504

Slope, I. (2006). *Digitilt inclinometer probe*. Durham Geo Slope Indicator.

Solari, L., Del Soldato, M., Raspini, F., Barra, A., Bianchini, S., Confuorto, P., Casagli, N., & Crosetto, M. (2020). Review of satellite interferometry for landslide detection in Italy. *Remote Sensing*, *12*(8), 1351. https://doi.org/10.3390/rs12081351

Song, C., Yu, C., Li, Z., Pazzi, V., Del Soldato, M., Cruz, A., & Utili, S. (2021). Landslide geometry and activity in Villa de la Independencia (Bolivia) revealed by InSAR and seismic noise measurements. *Landslides*, *18*(8), 2721–2737. https://doi.org/10.1007/s10346-021-01659-9

Stark, T. D., & Choi, H. (2008). Slope inclinometers for landslides. *Landslides*, *5*, 339–350. https://doi.org/10.1007/s10346-008-0126-3

Thompson, A. A. (2015). Overview of the RADARSAT constellation mission. *Canadian Journal of Remote Sensing*, *41*(5), 401–407. https://doi.org/10.1080/07038992.2015.1104633

Tofani, V., Raspini, F., Catani, F., & Casagli, N. (2013). Persistent Scatterer Interferometry (PSI) technique for landslide characterization and monitoring. *Remote Sensing*, *5*(3), 1045–1065. https://doi.org/10.3390/rs5031045

Tomás, R., Romero, R., Mulas, J., Marturià, J. J., Mallorquí, J. J., Lopez-Sanchez, J. M., Herrera, G., Gutiérrez, F., González, P. J., & Fernández, J. (2014). Radar interferometry techniques for the study of ground subsidence phenomena: A review of practical issues through cases in Spain. *Environmental Earth Sciences*, *71*(1), 163–181. https://doi.org/10.1007/s12665-013-2422-z

Torres, R., Snoeij, P., Geudtner, D., Bibby, D., Davidson, M., Attema, E., Potin, P., Rommen, B., Floury, N., & Brown, M. (2012). GMES Sentinel-1 mission. *Remote Sensing of Environment*, *120*, 9–24. https://doi.org/10.1016/j.rse.2011.05.028

Trigila, A., Iadanza, C., Bussettini, M., Lastoria, B., Barbano, A., & Munafò, M. (2021). *Dissesto idrogeologico in Italia: Pericolosità e indicatori di rischio* (Rapporto 356). ISPRA.

Trigila, A., Iadanza, C., & Spizzichino, D. (2010). Quality assessment of the Italian Landslide Inventory using GIS processing. *Landslides*, *7*(4), 455–470. https://doi.org/10.1007/s10346-010-0213-0

Turner, A. K. (2018). Social and environmental impacts of landslides. *Innovative Infrastructure Solutions*, *3*, 1–25. https://doi.org/10.1007/s41062-018-0175-y

Uzielli, M., Catani, F., Tofani, V., & Casagli, N. (2015). Risk analysis for the Ancona landslide—II: Estimation of risk to buildings. *Landslides*, *12*(1), 83–100. https://doi.org/10.1007/s10346-014-0477-x

Cruden, D. M., & Varnes, D. J. (1996). *Landslide types and processes. Landslides: Investigation and mitigation*. National Research Council (Transportation Research Board special report 247).

Virelli, M., Coletta, A., & Battagliere, M. L. (2014). ASI COSMO-SkyMed: Mission overview and data exploitation. *IEEE Geoscience Remote Sensing Magazine*, *2*(2), 64–66. https://doi.org/10.1109/MGRS.2014.2317837

Wasowski, J., & Bovenga, F. (2014). Investigating landslides and unstable slopes with satellite Multi Temporal Interferometry: Current issues and future perspectives. *Engineering Geology*, *174*, 103–138. https://doi.org/10.1016/j.enggeo.2014.03.003

Wasowski, J., & Pisano, L. (2020). Long-term InSAR, borehole inclinometer, and rainfall records provide insight into the mechanism and activity patterns of an extremely slow urbanized landslide. *Landslides*, *17*, 445–457. https://doi.org/10.1007/s10346-019-01276-7

WP/WLI, International Geotechnical Society, UNESCO, & Working Party for World Landslide Inventory. (1993). *Multilingual landslide glossary*. BiTech Publishers.

Yagüe-Martínez, N., Prats-Iraola, P., Gonzalez, F. R., Brcic, R., Shau, R., Geudtner, D., Eineder, M., & Bamler, R. (2016). Interferometric processing of Sentinel-1 TOPS data. *IEEE Transactions on Geoscience and Remote Sensing*, *54*(4), 2220–2234. https://doi.org/10.1109/TGRS.2015.2497902

Yu, L., Yan, C., Guo, S., Li, H., Tan, J., Liu, G., Xu, C., & Liu, Y. (2023). Mechanism analysis of Zulongding landslide on gentle piedmont slope: A creeping landslide triggered by rainfall. *Natural Hazards*, *118*(2), 1211–1234. https://doi.org/10.1007/s11069-023-06051-5